Biogeosciences, 15, 1447–1467, 2018
https://doi.org/10.5194/bg-15-1447-2018

Biogeosciences Open Access EGU

δ^{11}B as monitor of calcification site pH in divergent marine calcifying organisms

Jill N. Sutton[1], Yi-Wei Liu[1,2], Justin B. Ries[3], Maxence Guillermic[2], Emmanuel Ponzevera[4], and Robert A. Eagle[1,5,6]

[1]Université de Brest, UMR 6539 CNRS/UBO/IRD/Ifremer, LEMAR, IUEM, 29280, Plouzané, France
[2]Université de Brest, UMR 6539 CNRS/UBO/IRD/Ifremer, LGO, IUEM, 29280, Plouzané, France
[3]Department of Marine and Environmental Sciences, Marine Science Center, Northeastern University, 430 Nahant Rd, Nahant, MA 01908, USA
[4]Unité de Recherche Géosciences Marines, Ifremer, 29280, Plouzané, France
[5]Institute of the Environment and Sustainability, University of California, Los Angeles, LaKretz Hall, 619 Charles E Young Dr E no. 300, Los Angeles, CA 90024, USA
[6]Atmospheric and Oceanic Sciences Department, University of California, Los Angeles, Math Sciences Building, 520 Portola Plaza, Los Angeles, CA 90095, USA

Correspondence: Jill N. Sutton (jill.sutton@univ-brest.fr) and Robert A. Eagle (robeagle@g.ucla.edu)

Received: 20 April 2017 – Discussion started: 15 May 2017
Revised: 8 December 2017 – Accepted: 14 December 2017 – Published: 8 March 2018

Abstract. The boron isotope composition (δ^{11}B) of marine biogenic carbonates has been predominantly studied as a proxy for monitoring past changes in seawater pH and carbonate chemistry. However, a number of assumptions regarding chemical kinetics and thermodynamic isotope exchange reactions are required to derive seawater pH from δ^{11}B biogenic carbonates. It is also probable that δ^{11}B of biogenic carbonate reflects seawater pH at the organism's site of calcification, which may or may not reflect seawater pH. Here, we report the development of methodology for measuring the δ^{11}B of biogenic carbonate samples at the multi-collector inductively coupled mass spectrometry facility at Ifremer (Plouzané, France) and the evaluation of $\delta^{11}B_{CaCO_3}$ in a diverse range of marine calcifying organisms reared for 60 days in isothermal seawater (25 °C) equilibrated with an atmospheric pCO_2 of ca. 409 µatm. Average $\delta^{11}B_{CaCO_3}$ composition for all species evaluated in this study range from 16.27 to 35.09 ‰, including, in decreasing order, coralline red alga *Neogoniolithion* sp. (35.89 ± 3.71 ‰), temperate coral *Oculina arbuscula* (24.12 ± 0.19 ‰), serpulid worm *Hydroides crucigera* (19.26 ± 0.16 ‰), tropical urchin *Eucidaris tribuloides* (18.71 ± 0.26 ‰), temperate urchin *Arbacia punctulata* (16.28 ± 0.86 ‰), and temperate oyster *Crassostrea virginica* (16.03 ‰). These results are discussed in the context of each species' proposed mechanism of biocalcification and other factors that could influence skeletal and shell δ^{11}B, including calcifying site pH, the proposed direct incorporation of isotopically enriched boric acid (instead of borate) into biogenic calcium carbonate, and differences in shell/skeleton polymorph mineralogy. We conclude that the large inter-species variability in $\delta^{11}B_{CaCO_3}$ (ca. 20 ‰) and significant discrepancies between measured $\delta^{11}B_{CaCO_3}$ and $\delta^{11}B_{CaCO_3}$ expected from established relationships between abiogenic $\delta^{11}B_{CaCO_3}$ and seawater pH arise primarily from fundamental differences in calcifying site pH amongst the different species. These results highlight the potential utility of δ^{11}B as a proxy of calcifying site pH for a wide range of calcifying taxa and underscore the importance of using species-specific seawater-pH–$\delta^{11}B_{CaCO_3}$ calibrations when reconstructing seawater pH from δ^{11}B of biogenic carbonates.

1 Introduction

The ability to monitor historical changes in seawater pH on both short and long timescales is necessary to understand the influence that changes in the partial pressure of atmospheric CO_2 (pCO_2) have had on the carbonate chemistry of seawater. The recent anthropogenic increase in pCO_2 has already

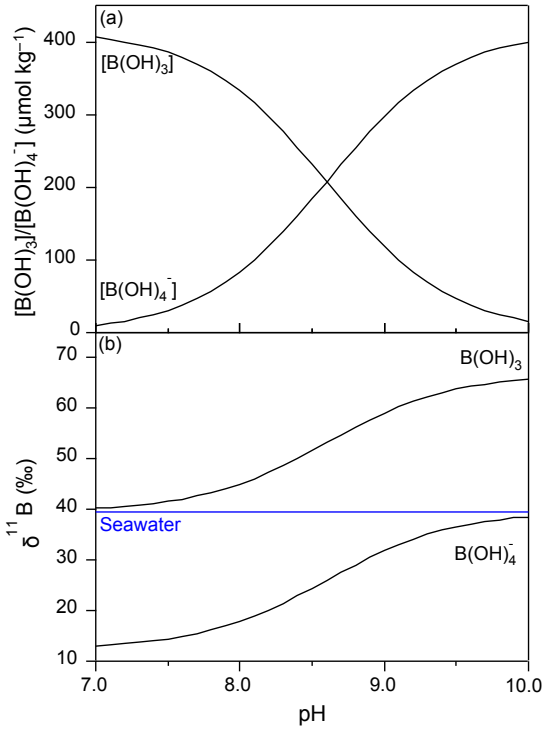

Figure 1. (a) Speciation of dissolved inorganic boron, $B(OH)_3$ and $B(OH)_4^-$, as a function of seawater pH. **(b)** δ^{11}B of dissolved inorganic boron species as a function of seawater pH. The pK_B is 8.6 at 25 °C and 35 psu (practical salinity units; Dickon, 1990), α is 1.0272 (Klochko et al., 2006), and $\delta^{11}B_{SW}$ is 39.61 (Foster et al., 2010).

resulted in a significant decrease in seawater pH (Bates, 2007; Byrne et al., 2010; Dore et al., 2009; Feely et al., 2008, 2016; Gonzalez-Davlia et al., 2010; IPCC, 2014), which affects the ability of marine calcifying organisms to produce their shells and skeletons ($CaCO_3$; IPCC, 2014). Experimental studies have revealed that organismal responses to ocean acidification vary widely amongst taxa, highlighting the complexity of biological responses to global change stressors (e.g., Kroeker et al., 2010, 2013; Ries et al., 2009) and necessitating a more thorough understanding of how an organism's mechanism of biocalcification governs its specific response to ocean acidification.

1.1 Theoretical model of δ^{11}B variation with pH

The boron isotope composition (δ^{11}B) of biogenic $CaCO_3$ ($\delta^{11}B_{CaCO_3}$) has been primarily used as a paleoceanographic proxy for seawater pH (Hönisch and Hemming, 2004; Hönisch et al., 2004; Montagna et al., 2007; Palmer, 1998; Pearson et al., 2009; Penman and Hönisch, 2014; Rae et al., 2011; Trotter et al., 2011; Vengosh et al., 1991; Wei et al., 2009). Boron has a residence time in seawater of ca. 14 million years (Lemarchand et al., 2000), which is much longer than the mixing time of oceans (ca. 1000 years), suggesting that it is conservatively distributed throughout the ocean (Foster et al., 2010) – making δ^{11}B a potentially attractive proxy for paleo-seawater pH.

Boron exists in aqueous solutions as either trigonal boric acid $[B(OH)_3]$ or as the tetrahedral borate anion $[B(OH)_4^-]$, with the proportions of these two chemical species varying as a function of pH (Fig. 1) pursuant to the following equilibrium reaction:

$$B(OH)_3 + H_2O \leftrightarrow B(OH)_4^- + H^+.$$

In modern seawater, $B(OH)_4^-$ represents ca. 24.15 % of dissolved boron, assuming that the dissociation constant (pK_B) between the two species of boron is 8.597 (at 25 °C, pH = 8.1, 35 psu (practical salinity units); Dickson, 1990). Boron has two stable isotopes, ^{10}B and ^{11}B, with relative abundances of 19.9 and 80.1 %, respectively. $B(OH)_3$ is enriched in ^{11}B relative to $B(OH)_4^-$ due to differences in the ground state energy of molecular vibration of these chemical species in solution. The isotopic composition of boron is expressed following standard convention:

$$\delta^{11}B = \left[\frac{\left(\frac{^{11}B_{sample}}{^{10}B_{sample}}\right)}{\left(\frac{^{11}B_{standard}}{^{10}B_{standard}}\right)} - 1 \right] \times 1000\ (‰), \quad (1)$$

where the reference standard is NIST SRM (Standard Reference Materials) 951 (Catanzaro et al., 1970).

The δ^{11}B of modern seawater is 39.61 ± 0.20 ‰ (Foster et al., 2010) and a large (> 20 ‰) and constant isotope fractionation exists between the two aqueous species described above. The fractionation factor (α) for boric acid and borate ion is defined as follows:

$$\alpha = \frac{\left(^{11}B/^{10}B\right)_{Boric\ acid}}{\left(^{11}B/^{10}B\right)_{Borate\ ion}}.$$

A range of theoretical and empirical values for α has been suggested (Byrne et al., 2006; Kakihana et al., 1977; Klochko et al., 2006; Nir et al., 2015; Palmer et al., 1987). For example, α of 1.0194 was calculated from theory by Kakihana et al. (1977) and was widely applied in reconstructions of paleo-seawater pH (Hönisch et al., 2004; Kakihana et al., 1977; Sanyal et al., 1995). Zeebe (2005) used analytical techniques and ab initio molecular orbital theory to calculate α ranging from 1.020 to 1.050 at 300 K. Zeebe (2005) provided several arguments in support of $\alpha \geq 1.030$, ultimately concluding that experimental work was required to determine the α for dissolved boric acid and the borate ion. Subsequent to the work by Zeebe (2005), significant error was identified for the borate vibrational spectrum term used in Kakihana et al.'s (1977) theoretical calculation of α (Klochko et al., 2006; Rustad and Bylaska, 2007). An empirical α of 1.0272 (Klochko et al., 2006), using a corrected borate vibrational

spectrum term, is now considered to best describe the boron isotope fractionation between dissolved boric acid and borate ion in seawater (Rollion-Bard and Erez, 2010; Xiao et al., 2014). Moreover, due to the ability of some calcifying organisms to alter carbonate chemistry at their site of calcification, paleo-seawater pH cannot always be reliably reconstructed simply by projecting measured δ^{11}B of calcium carbonate ($\delta^{11}B_{CaCO_3}$) onto a theoretical seawater borate δ^{11}B ($\delta^{11}B_{B(OH)_4^-}$)–pH curve (see also Anagnostou et al., 2012; Honïsch et al., 2003; Sanyal et al., 1996, 2001; Trotter et al., 2011). Instead, the species used for paleo-seawater pH reconstructions may require calibration through controlled laboratory experiments and/or core-top calibrations that empirically define the species-specific relationship between seawater pH (pH_{SW}) and $\delta^{11}B_{CaCO_3}$.

The δ^{11}B-based paleo-seawater pH proxy is based on a theoretical model of $\delta^{11}B_{B(OH)_4^-}$ variation with pH described by the following equation (Zeebe and Wolf-Gladrow, 2001):

$$\mathrm{pH} = \mathrm{pK_B} - \log\left(\frac{\delta^{11}B_{CaCO_3} - \delta^{11}B_{SW}}{\delta^{11}B_{SW} - \left(\alpha_B \times \delta^{11}B_{CaCO_3}\right) - 1000\,(\alpha - 1)}\right).$$

This theoretical model of $\delta^{11}B_{B(OH)_4^-}$ variation as a function of seawater pH requires knowledge of the α for isotope exchange between the aqueous species of boron, the dissociation constant (pK_B), and the isotopic composition of total boron in seawater (Pagani et al., 2005) – each of which can introduce uncertainty into the pH reconstruction.

Application of this proxy also assumes that $\delta^{11}B_{CaCO_3}$ reflects seawater $\delta^{11}B_{B(OH)_4^-}$ and, thus, seawater pH (Hemming and Hanson, 1992). Although early studies assumed that $\delta^{11}B_{CaCO_3}$ was indeed equivalent to seawater $\delta^{11}B_{B(OH)_4^-}$ (e.g., Hemming and Hanson, 1992), Sanyal et al. (2000, 2001) observed that empirically derived $\delta^{11}B_{CaCO_3}$–pH curves of biogenic and abiogenic calcites were parallel but vertically offset from the theoretical $\delta^{11}B_{B(OH)_4^-}$–pH curve, which led them to conclude that paleo-seawater pH cannot always be directly calculated from $\delta^{11}B_{CaCO_3}$ using the theoretical $\delta^{11}B_{B(OH)_4^-}$–pH relationship (i.e., $\delta^{11}B_{CaCO_3}$–pH relationships must be empirically calibrated for the species hosting the paleo-pH proxy).

The δ^{11}B-based paleo-seawater pH proxy also relies on the assumption that $B(OH)_4^-$ is the dominant species of dissolved inorganic boron incorporated into $CaCO_3$ minerals precipitated from seawater. It is well established that δ^{11}B of dissolved $B(OH)_4^-$ is controlled by solution pH (cf. Hemming and Hönisch, 2007; see discussion above). Therefore, $\delta^{11}B_{CaCO_3}$ should reflect pH of the precipitating solution if $B(OH)_4^-$ is indeed the dominant species of dissolved inorganic boron incorporated into $CaCO_3$, which is consistent with numerous empirical studies (see Hemming and Hönisch, 2007, for summary).

More recently, however, alternative models of boron incorporation into $CaCO_3$ have been proposed (Balan et al., 2016; Klochko et al., 2009; Noireaux et al., 2015; Uchikawa et al., 2015). These studies present evidence consistent with the incorporation of boric acid, along with borate, into some carbonates (e.g., Noireaux et al., 2015; Uchikawa et al., 2015) and/or the occurrence of trigonal boron in the carbonate lattice due to transformation from borate during carbonate precipitation (e.g., Mavromatis et al., 2015). Some of these studies also suggest that calcite is more prone to boric acid incorporation than aragonite (e.g., Noireaux et al., 2015). These alternative models pose a potential challenge to the utility of boron isotopes in reconstructing calcifying fluid and paleo-seawater pH (Balan et al., 2016; Klochko et al., 2009; Mavromatis et al., 2015; Noireaux et al., 2015; Uchikawa et al., 2015). Some of these studies also suggest that calcite is more prone to boric acid incorporation than aragonite (e.g., Noireaux et al., 2015). However, these studies evaluated inorganic carbonate precipitates from fluids of compositions that differed substantially from seawater; it is yet to be determined whether boric acid incorporation is equally as prevalent in carbonates that are precipitated from seawater. Nevertheless, we evaluate boric acid incorporation as an alternative to the hypothesis that calcifying fluid pH exerts primary control over the δ^{11}B composition of most biogenic carbonates.

1.2 The role of calcification site pH in calcareous biomineralization and organisms' responses to ocean acidification

Many calcifying marine organisms, including scleractinian corals (Al-Horani et al., 2003; Cohen and Holcomb, 2009; Cohen and McConnaughey, 2003; Rollion-Bard et al., 2003, 2011b; Holcomb et al., 2010; Krief et al., 2010; Trotter et al., 2011; Ries, 2011a; Anagnostou et al., 2012; McCulloch et al., 2012; Wall et al., 2016), coralline red algae (Borowitzka and Larkum, 1987; McConnaughey and Whelan, 1997; Donald et al., 2017), calcareous green algae (Borowitzka and Larkum, 1987; De Beer and Larkum, 2001; McConnaughey and Falk, 1991), foraminifera (Rink et al., 1998; Zeebe and Sanyal, 2002), and crabs (Cameron, 1985) are thought to facilitate precipitation of their skeletal or shell $CaCO_3$ by elevating the pH at their site of calcification. The effect of pH on $CaCO_3$ chemistry at the site of calcification can be summarized by the following equilibrium reactions:

$$H_2CO_3 \leftrightarrow HCO_3^- + H^+$$

and

$$HCO_3^- \leftrightarrow H^+ + CO_3^{2-},$$

which are respectively governed by the following stoichiometric dissociation constants:

$$K_1^* = \left[HCO_3^-\right]\left[H^+\right] / \left[H_2CO_3\right]$$

and

$$K_2^* = \left[CO_3^{2-}\right]\left[H^+\right] / \left[HCO_3^-\right].$$

Thus, reducing $[H^+]$ at the site of calcification shifts the carbonic acid system towards elevated $[CO_3^{2-}]$, thereby increasing the $CaCO_3$ saturation state (Ω_{CaCO_3}) following

$$\Omega_{CaCO_3} = \left[Ca^{2+}\right]\left[CO_3^{2-}\right]/K^*_{sp},$$

where K^*_{sp} is the stoichiometric solubility product of the appropriate $CaCO_3$ polymorph (e.g., calcite, aragonite) and is influenced by temperature, pressure, and salinity.

The decrease in pH_{SW} that will accompany the rise in anthropogenic atmospheric pCO_2 will reduce seawater $[CO_3^{2-}]$, which has been shown to inhibit biological deposition of $CaCO_3$, or even promote its dissolution (cf. Doney et al., 2009; Fabry et al., 2008; Kleypas et al., 2006; Kroeker et al. 2010; Langdon, 2002; Ries et al., 2009, 2016). However, if seawater is the source of an organism's calcifying fluid (e.g., Gaetani and Cohen, 2006), then the concentration of dissolved inorganic carbon (DIC) in this fluid will increase as atmospheric pCO_2 increases. Organisms able to strongly regulate pH of their calcifying fluid (pH_{CF}), despite reduced external pH, should convert much of this increased DIC, occurring primarily as HCO_3^-, back into the CO_3^{2-} needed for calcification (Ries, 2011a, b; Ries et al., 2009). Thus, an organism's specific response to CO_2-induced ocean acidification should be strongly dependent upon that organisms' ability to regulate pH at their site of calcification.

Marine calcifiers biomineralize in diverse ways, with some calcifers' mechanisms of biomineralization better understood than others. Corals are thought to accrete $CaCO_3$ directly from a discrete calcifying fluid (e.g., Al-Horani et al., 2003; Cohen and Holcomb, 2009; Cohen and McConnaughey, 2003 and references therein; Gaetani and Cohen, 2006; Ries, 2011a), with mineralization sites and crystal orientations being influenced by organic templates and/or calicoblastic cells (e.g., Cuif and Dauphin, 2005; Goldberg, 2001; Meibom et al., 2008; Tambutté et al., 2007). Mollusks are also thought to precipitate their shells from a discrete calcifying fluid between the external epithelium of the mantle and the inner layer of the shell known as the extrapallial fluid (EPF; e.g., Crenshaw, 1972), with hemocytes and organic templates playing a potentially important role in crystal nucleation (e.g., Marie et al., 2012; Mount et al., 2004; Weiner et al., 1984). Coralline red algae are also thought to precipitate primarily high-Mg calcite (HMC) extracellularly but within a chemically controlled fluid bound by adjacent cells. Echinoids, in contrast, are thought to initiate calcification on Ca^{2+}-binding organic matrices within cellular vacuoles (Ameye et al., 1998).

Various mechanisms have been proposed for elevating pH_{CF}, including conventional H^+ channelling (McConnaughey and Falk, 1991), Ca^{2+}–H^+ exchanging ATPase (Cohen and McConnaughey, 2003; McConnaughey and Falk, 1991; McConnaughey and Whelan, 1997), light-induced H^+ pumping (De Beer and Larkum, 2001), transcellular symporter and co-transporter H^+-solute shuttling (McConnaughey and Whelan, 1997), cellular extrusion of hydroxyl ions (OH^-) into the calcifying medium, and CO_2 consumption via photosynthesis (e.g., Borowitzka and Larkum, 1976).

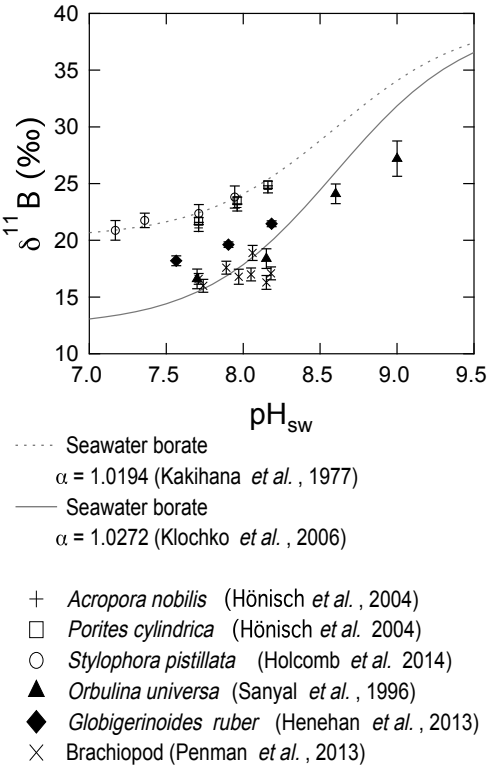

Figure 2. Examples of previously published $\delta^{11}B_{CaCO_3}$–pH_{SW} trends for corals, foraminifera, and brachiopods. Although many B isotope data sets are available, only studies with ≥ 3 $\delta^{11}B_{CaCO_3}$–pH_{SW} data spanning a sufficiently wide range of pH_{SW} conditions were selected to illustrate the range of $\delta^{11}B_{CaCO_3}$–pH_{SW} trends published to date. The two grey lines correspond to the theoretical seawater borate δ^{11}B–pH curves that have been applied most frequently to interpret δ^{11}B variability in marine calcifiers and were generated using a pK_B of 8.6 at 25 °C and 35 psu (Dickson, 1990).

Regardless of the exact composition (e.g., seawater vs. modified seawater) or nature (e.g., fluid vs. gel) of its calcifying medium, or the specific mechanisms by which it produces $CaCO_3$ (e.g., organic templates vs. cellular mediation vs. proton pumps vs. Ca^{2+} ATPase), an organism's ability to control pH_{CF} should strongly influence its ability to convert DIC into CO_3^{2-}, thereby impacting its specific calcification response to CO_2-induced ocean acidification.

1.3 Relationship between calcification site pH and $\delta^{11}B_{CaCO_3}$

Numerous studies have documented systematic relationships between pH_{SW} and the $\delta^{11}B_{CaCO_3}$ composition of foraminiferal shells and coral skeletons (Fig. 2) that are gen-

erally consistent with theoretically derived relationships between seawater pH and $\delta^{11}B_{B(OH)_4^-}$. However, the observed relationships between biogenic $\delta^{11}B_{CaCO_3}$ and pH_{SW} vary widely amongst taxa (Fig. 2) and are generally offset from that measured or derived theoretically for $B(OH)_4^-$ in seawater (Byrne et al., 2006; Klochko et al., 2006; Liu and Tossell, 2005; Zeebe, 2005) and from that observed in abiotically precipitated $CaCO_3$ (Noireaux et al., 2015; Sanyal et al., 2000).

One hypothesis for the discrepancies between the expected $\delta^{11}B_{CaCO_3}$–pH relationship and those actually observed for biogenically precipitated $CaCO_3$ is that most marine calcifiers are not precipitating their $CaCO_3$ directly from seawater, but rather from a discrete calcifying fluid with a pH (pH_{CF}) that is substantially elevated relative to that of their external seawater (pH_{SW}). For example, prior studies have shown that for a given pH_{SW}, $\delta^{11}B_{CaCO_3}$ of the coral species *Porites cylindrica* and *Acropora nobilis* are moderately elevated relative to $\delta^{11}B_{CaCO_3}$ of the foraminifera *Globigerinoides sacculifer* and substantially elevated relative to $\delta^{11}B_{CaCO_3}$ of the mussel *Mytilus edulis* (Fig. 2; Heinemann et al., 2012; Hönisch et al., 2004; Sanyal et al., 2001). One possible explanation for these differences is that corals are maintaining their calcifying fluids at higher pH than the calcifying fluids of foraminifera, which are in turn elevated relative to the pH_{CF} of mussels. This is consistent with pH microelectrode and pH-sensitive fluorescent dye data (Venn et al., 2009, 2011, 2013), showing that, compared to their external pH_{SW} of 8, scleractinian corals elevate their pH_{CF} to 8.5–10 (Al-Horani et al., 2003; Ries, 2011a; Venn et al., 2009, 2011, 2013), that foraminifera maintain their pH_{CF} between 8 and 9 (Jorgensen et al., 1985; Rink et al., 1998), and that bivalves maintain their pH_{CF} between 7.5 and 8 (Crenshaw, 1972).

Here, we investigate differences in $\delta^{11}B_{CaCO_3}$–pH relationships amongst taxonomically diverse biogenic calcification systems and discuss the compatibility of these observations with the hypothesis that $\delta^{11}B_{CaCO_3}$ of biogenic carbonate is recording pH_{CF} (rather than pH_{SW}) – a key parameter of biological calcification that has proven challenging to measure yet is fundamental to understanding, and even predicting, marine calcifiers' responses to CO_2-induced ocean acidification. By systematically investigating the $\delta^{11}B_{CaCO_3}$ composition of a taxonomically broad range of taxa, each employing different mechanisms of calcification yet all cultured under equivalent laboratory conditions (Ries et al., 2009), we are able to empirically assess biological controls on the $\delta^{11}B_{CaCO_3}$ composition of biogenic carbonates.

2 Methods and materials

2.1 Laboratory conditions

Sample processing and chemical separation were performed under ISO 5 (class 100) laminar flow hoods within an ISO 6 (class 1000) clean room at Ifremer (Plouzané, France). Analyses of ^{11}B / ^{10}B ratios were carried out using a Thermo Scientific Neptune MC-ICPMS (multi-collector inductively-coupled plasma mass spectrometer) at the Pôle Spectrometrie Océan (PSO), Ifremer (Plouzané, France). Efforts were made to minimize sample exposure to laboratory air by, for example, removing caps of sample vials only when reagents were added to the samples and just prior to sample analysis.

2.2 Reagents

Ultra-pure reagents were used for all chemical procedures. The source of high-purity water (UHQ) for the procedures was a Millipore Direct-Q water purification system with a specific resistivity of 18.2 MΩ·cm. All HNO_3 solutions are obtained from dilutions using Aristar ultra-high-purity acid. The 0.5 N NH_4OH solutions are boron cleaned by exchange with boron-specific resin (Amberlite IRA 743). UHQ water is buffered to pH 7 with the boron-cleaned NH_4OH. The reagent boron blanks were measured on a Thermo Scientific Element XR at the PSO, Ifremer (Plouzané, France), and were all < 0.1 ppb, yielding a total B blank of < 100 ng per sample.

2.3 Materials

2.3.1 Samples

This study evaluated the $\delta^{11}B_{CaCO_3}$ of six divergent species of marine calcifiers reared for 60 days in isothermal (25 °C) and isosaline (32 psu) seawater equilibrated with atmospheric pCO_2 of ca. 409 µatm, including a temperate coral (*Oculina arbuscula*), a tropical coralline red alga (*Neogoniolithion* sp.), a tropical urchin (*Eucidaris tribuloides*), a temperate urchin (*Arbacia punctulata*), a serpulid worm (*Hydroides crucigera*), and a temperate oyster (*Crassostrea virginica*; see Ries et al., 2009, for details). The specimens were subsampled for new growth relative to a barium marker emplaced at the start of the experiment (details in Ries, 2011), homogenized, and at least three specimens per species analyzed for $\delta^{11}B_{CaCO_3}$.

2.3.2 Standards

A range of standards were used in this study, including (1) the reference standard NIST SRM 951 (Catanzaro et al, 1970) for δ^{11}B and B concentration, (2) a mixture of NIST SRM 951 and a series of ICPMS SRM for the B : Ca ratio (30–200 µg mg^{-1}), (3) the international coral standard (*Porites* sp.) JCp-1 (Geological Survey of Japan, Tsukuba, Japan), (4) the international giant clam standard (*Tridacna gigas*) JCt-1 (Geological Survey of Japan, Tsukuba, Japan), and (5) a laboratory coral standard (NEP; *Porites* sp.) from the University of Western Australia and the Australian National University (McCulloch et al., 2014).

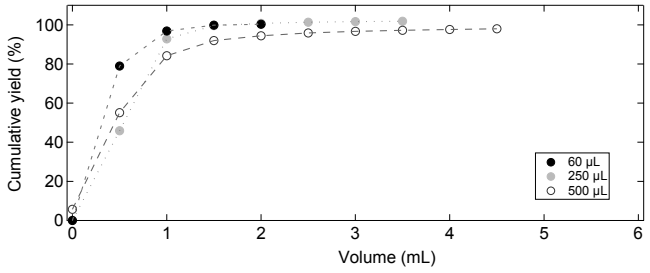

Figure 3. Elution curves indicating cumulative yield of boron for different volumes of the boron-specific resin (Amberlite IRA 743) used in the ion exchange column.

2.4 Boron extraction procedure

Prior to boron isotope analysis, B was separated from the sample matrix using a B-specific anionic exchange resin (Amberlite IRA-743; Kiss, 1988). Amberlite IRA 743 functions as an anion exchanger with a high affinity for B absorption at neutral to alkaline pH (i.e., will absorb B) and a low affinity for boron at acidic pH (i.e., will release B). The resin was crushed and sieved to a desired 100–200 mesh size, then cleaned and conditioned to a pH of 7 (6.8–7.2).

Two methods of B extraction are presented: batch and column chemistry. For both, the influence of matrix chemistry is removed through minor adjustments to the chemistry of existing B extraction techniques. These two methods were applied to four biogenic $CaCO_3$ samples (*Porites* coral standard, temperate urchin, giant clam, American oyster).

2.4.1 Oxidative cleaning

Samples and reference materials JCp-1, JCt-1, and NEP were cleaned with an oxidative cleaning method following the method of Barker et al. (2003). For a 2 mg sample, 200 µL of the alkaline-buffered (0.1 M NH_4OH) H_2O_2 was added to remove organic matter. Samples were placed in an ultrasonicator for 20 min at 50 °C to expedite cleaning. After peroxide cleaning, samples were submitted to multiple washes (typically three) of UHQ water (pH = 7, 400 µL) until the pH of the supernatant matched that of the UHQ water, which ensured removal of all of the oxidizing agent. The water was then removed from samples after centrifugation and a weak-acid leach was implemented by adding 20 µL of 0.001 M HNO_3 to each sample. Samples were then ultrasonicated for 10 min, centrifuged, and separated from the acid. The samples were washed twice with pH-buffered UHQ water (buffered to pH 7 with 2 % NH_4OH), centrifuged, and then separated from the water. Dissolution of each sample was then performed by addition of 20 µL of 3 M HNO_3, followed by addition of 300 µL of 0.05 M HNO_3. The pH of each sample was then adjusted to pH 7 with 0.2 M NH_4OH, following distribution coefficients for the B-specific resin reported by Lemarchand et al. (2002).

Table 1. Protocol used to evaluate the column chemistry method of boron extraction. Three volumes of resin (60, 250, and 500 µL) were evaluated.

Step	mg resin	15	62.5	125
1	Resin (µL)	60	250	500
2	UHQ H_2O at pH 7 (mL)	5	5	5
3	0.5 N HNO_3 (mL)	2.5	2.5	5
4	UHQ H_2O at pH 7 (mL) ×3	2.5	2.5	5
5	Check pH			
6	Sample Load (ng)	536	536	536
7	UHQ H_2O at pH 7 (mL) ×3	1	1	2
8	Check pH			
9	0.05 N HNO_3 (mL)	0.5	0.5	0.5
10	UHQ H_2O at pH 7 (mL)	2	2	2

2.4.2 Column chemistry method

A column chemistry protocol for B extraction (described in Table 1) was developed based on methods described by Wang et al. (2010) and Foster et al. (2013). Briefly, the columns were washed with pH-buffered UHQ H_2O (pH=7), 0.5 M HNO_3, and again with pH-buffered UHQ H_2O. After confirming that the eluent was at pH 7, the sample was loaded onto the resin and washed multiple times (1500 µL × 3) with pH-buffered UHQ in order to remove any cations, after which the B was eluted in 1000 µL of 0.5 M HNO_3. Column yields were greater than 95 % (Fig. 3) and elution tails of every sample were checked with an additional 500 µL acid rinse. In all cases, this tail represented less than 1 % of B loaded. Small aliquots of each sample were measured by single-collector HR-ICPMS (high-resolution ICPMS) prior to analysis by MC-ICPMS to verify retention of B on the column and removal of other elements (e.g., Ca, Na, Ba, U).

2.4.3 Batch method

The batch method approach to B separation was conducted under closed conditions in order to reduce airborne B contamination. Cleaned samples (pH 7) were transferred into acid-cleaned microcentrifuge tubes (500 µL; polypropylene) containing 5 mg of resin (see Sect. 2.4), which is B cleaned in individual tubes with 500 µL of 0.5 M HNO_3, and then rinsed three times with 500 µL of UHQ water to elute the other cations in the matrix and achieve pH 7. Tubes were then capped and shaken for 15 min to promote exchange of anions from the aqueous sample to the resin. Afterwards, the mixture was centrifuged (1 min, 2000 rpm), the matrix was decanted, and the resin was washed three times (200 µL) with pH-buffered (pH 7) UHQ water to elute any cations. Boron recovery was then performed with the addition of 500 µL 0.05 M HNO_3 and shaken again for 15 min to promote anion exchange between the resin and solution. A final tail check was performed with 100 µL of 0.05 M HNO_3 to ensure that

all of the B was recovered in the initial 500 µL 0.05 M HNO_3 solution.

2.5 Procedural blanks

The total yield of B from procedural blanks, which should reflect reagent, airborne and procedural contamination, was sub-nanogram (lowest yields for column and batch methods were 0.5 ng and 90 pg, respectively). Such low contamination was achieved through stringent cleaning and handling protocols for all consumables and reagents, thereby permitting accurate measurement of B at sub-µM concentrations.

2.6 Boron recovery and matrix removal

A major challenge in the measurement of δ^{11}B by MC-ICPMS is the elimination of residual boron from prior analyses (i.e., memory effects). In order to evaluate memory effects, multiple concentrations (30 to 130 ppb) of a standard solution (NIST SRM 951) were analyzed. After washing out the MC-ICPMS with a solution of 0.05 M HNO_3 for several minutes, the residual ^{11}B and ^{10}B signals were in the range of 10–80 mV, equivalent to 5 % (30 ppb) and 3 % (130 ppb), respectively (see Fig. S1 in the Supplement for ^{11}B blanks). Boron recovery was measured using a Thermo Scientific Element XR HR-ICP-MS at the Laboratory for Geochemistry and Metallogeny, Ifremer (Plouzané, France). Boron yields are evaluated by tracking B throughout the entire procedure.

2.7 Mass spectrometry

Isotopic measurements were conducted using a Thermo Scientific Neptune MC-ICPMS at the PSO, Ifremer (Plouzané, France), operated with standard plasma settings. To account for drift in mass discrimination through the analysis, samples were bracketed by matrix-matched standards of similar composition. Typically, the concentration of the standard (NIST SRM 951) was 50 ppb in 0.05 M HNO_3. Each analysis consisted of a 2 min simultaneous collection of masses 11 and 10 on Faraday cups H3 and L3 equipped with $10^{11}\,\Omega$ resistors. Each sample was analyzed in duplicate during a single analytical session, with replicate analyses not sharing a bracketing standard. The boron isotope ratios are reported as delta values (δ^{11}B). The δ^{11}B of the calcium carbonate standards JCp-1 (*Porites* sp.), NEP (*Porites* sp.), and JCt-1 (hard clam) standards were processed in the same manner and are reported in the results section (see Sect. 3.1.1) alongside their published reference values (Foster et al., 2013; McCulloch et al., 2014).

The MC-ICPMS is commonly used to measure δ^{11}B due to its capacity for rapid, accurate, and reproducible analyses (see McCulloch et al., 2014, for a recent summary of these methods). Challenges with this method arise from the volatile and persistent nature of boron that can result in significant memory effects, cross-contamination between samples and standards, and unanticipated matrix effects (McCulloch et al., 2014; Foster et al., 2013). Given the sensitivity of $\delta^{11}B_{CaCO_3}$-based estimates of pH_{CF} to the analytical uncertainty cited above, two different injection methods (described below) were evaluated to determine which is most suitable for minimizing analytical error.

2.7.1 Demountable direct injection nebulizer

Memory effects, as described above in Sect. 2.7, were addressed by introducing samples to the plasma with a demountable direct injection high-efficiency nebulizer (*d*-DIHEN; Louvat et al., 2014). The *d*-DIHEN method minimizes the influence of memory effects by eliminating the use of a spray chamber and directly injecting the sample into the plasma (see Louvat et al., 2014, for details). Baseline B concentrations between samples were measured with counting times of 30 s (Table 2).

2.7.2 Ammonia addition

For the ammonia-addition method, a dual-inlet PFA Teflon spray chamber was used with an ESI PFA 50 µL min^{-1} nebulizer to add ammonia gas at a rate of ca. 3 mL min^{-1} (Al-Ammar et al., 2000; Foster, 2008). The addition of ammonia gas to the spray chamber ensures that the analyte remains alkaline, which prevents volatile boron from recondensing in the chamber during analysis (Al-Ammar et al., 2000). The measured B isotope signal of the rinse blank was then subtracted from the B isotope ratios in order to monitor B washout, as suggested by Foster (2008). In all cases, washout time was 200 s and samples were matrix- and intensity-matched to the bracketing standards.

3 Results

3.1 Method development

The yields for boron extraction for both methods were evaluated for various biogenic $CaCO_3$ samples and were typically between 97 and 102 % (determined by HR-ICPMS; see Sect. 2.6). Washes with pH-buffered UHQ H_2O effectively removed Ca (99.9 %), Na (100 %), Ba (> 80 %), and U (> 93 %) from the sample matrix. The robustness of the methods is demonstrated by the observed agreement (represented as 2 standard deviations around the mean; "2SD") between measured values of the international $CaCO_3$ standards JCp-1 (a *Porites* sp. coral; $\delta^{11}B_{NH_3} = 24.45 \pm 0.28$ ‰, $\delta^{11}B_{d-DIHEN} = 24.30 \pm 0.16$ ‰) and JCt-1 (the giant clam *Tridacna gigas*; $\delta^{11}B_{NH_3} = 16.65 \pm 0.39$ ‰, $\delta^{11}B_{d-DIHEN} = 17.5 \pm 0.69$ ‰), and their values established via inter-laboratory calibration ($\delta^{11}B = 24.36 \pm 0.51$ ‰, $n = 10$ and 16.34 ± 0.64 ‰; Gutjahr et al., 2014; see Table 3). In addition, both column and batch methods were evaluated using the NEP laboratory standard (*Porites* sp.), a temperate urchin, a hard clam, and an oyster. As shown in

Table 2. Mass spectrometer operating conditions.

	d-DIHEN	Ammonia addition
Injection system	Demountable Direct Injection High-Efficiency Nebulizer	PFA Teflon spray chamber with ESI PFA Teflon 50 µL min^{-1} nebulizer
Sample gas flow rate	0.3 L min^{-}	1.1 L min^{-1}
Running concentrations	B = 50 ppb	B = 30–50 ppb (evaluated 30, 65, 130 ppb)
Sensitivity	35 V ppm^{-1}, total B	20 V ppm^{-1}, total B
Blank level	< 0.5 % of ^{11}B signal after 30s in 2 % HNO_3, 0.1 % after 120 s	< 5 % of ^{11}B signal after 30 s in 0.05 % HNO_3, 3 % after 120 s
Resolution	Low	Low
Forward power	1200 W	1200 W
Accelerating voltage	10 kV	10 kV
Plasma mode	Wet plasma	Wet plasma
Cool gas flow rate	16 L min^{-1}	16 L min^{-1}
Auxiliary gas flow rate	0.9 L min^{-1}	0.9 L min^{-1}
Sampler cone	Standard Ni cone	Standard Ni cone
Skimmer cone	X Ni cone	X Ni cone
Interferences	$^{40}Ar^{++++}$ $^{20}Ne^{++}$ resolved	$^{40}Ar^{++++}$ $^{20}Ne^{++}$ resolved
Accuracy	0.2 ‰ , 2sd, $n = 6$	0.2 ‰, 2sd, $n = 6$
Acquisition	30 × 4 s	30 × 4 s
Baselines	Counting times of 20 s	Counting times of 20 s

Table 3, good agreement was achieved between $\delta^{11}B_{CaCO_3}$ obtained via the batch and column chemistry methods for each of the biogenic $CaCO_3$ samples analyzed.

3.2 Boron isotope composition of marine biogenic $CaCO_3$

Average $\delta^{11}B_{CaCO_3}$ composition for all species evaluated in this study range from 16.27 to 35.09 ‰ (Table 3). The individual and average data are presented in Tables 3 and 4, respectively, and summarized in the text that follows. Note that the variance of the data presented in Table 4 represents interspecimen variability (i.e., variability amongst different specimens of the same species), which is substantially greater than the intra-specimen variability (i.e., variability within a specimen) and analytical variability (variability amongst repeat analyses of the same subsample of a specimen; Table 3). The coralline red alga *Neogoniolithion* sp. (35.89 ± 3.71 ‰; $n = 3$) exhibited the highest $\delta^{11}B_{CaCO_3}$, followed by the temperate coral *O. arbuscula* (24.12 ± 0.19 ‰; $n = 3$), the tube of the serpulid worm *H. crucigera* (19.26 ± 0.16 ‰; $n = 3$), the tropical urchin *E. tribuloides* (18.71 ± 0.26 ‰; $n = 3$), the temperate urchin *A. punctulata* (16.28 ± 0.86 ‰; $n = 3$), and the temperate oyster *C. virginica* (16.03 ‰; $n = 1$). Therefore, a range of ca. 20 ‰ in $\delta^{11}B_{CaCO_3}$ was observed across all species evaluated in this study (Tables 3 and 4). Notably, these are the first published $\delta^{11}B_{CaCO_3}$ data for serpulid worm tubes and oysters.

3.3 Compatibility of the interspecific range of $\delta^{11}B_{CaCO_3}$ with established seawater borate δ^{11}B–pH relationships

Because the investigated species were cultured under relatively equivalent conditions (pCO_2 of 409 ± 6 µatm, 32 ± 0.2 psu, 25 ± 0.1 °C; see Ries et al., 2009), differences in pH_{SW} could not have been a significant driver of the observed interspecific variability in $\delta^{11}B_{CaCO_3}$ (ca. 20 ‰; Tables 3 and 4). In order to evaluate this ca. 20 ‰ interspecific variability in δ^{11}B, the data are plotted against measured pH_{SW} and graphically compared with theoretical borate δ^{11}B–pH curves often used to interpret $\delta^{11}B_{CaCO_3}$ data in the context of pH_{SW} (Fig. 4). Clear offsets from the seawater borate δ^{11}B–pH curve (Klochko et al., 2006) can be observed for several of the species: the temperate coral (*O. arbuscula*) and coralline red alga (*Neogoniolithion* sp.) fall above the curve, the temperate urchin (*A. punctulata*) and American oyster (*C. virginica*) fall below the curve, and the tube of the serpulid worm (*H. crucigera*) and the tropical urchin (*E. tribuloides*) fall nearly on the curve (see Fig. 4 and Table 3). The interpretation of these offsets from the seawater borate δ^{11}B–pH curve is presented below.

4 Discussion

4.1 Appropriateness of method for analyzing $\delta^{11}B_{CaCO_3}$ in marine $CaCO_3$ samples

This study describes extensive method development and analytical validation used to establish stable boron isotope mea-

Table 3. Boron isotope composition (δ^{11}B; ‰) of all species evaluated, including international carbonate standards JCp-1 (coral, *Porites* sp.) and JCt-1 (giant clam, *Tridacna gigas*). Data are presented as the average of n analyses and the precision is reported as 2 standard deviations (2SD). The cleaning protocol (oxidized, Ox; uncleaned, U), separation method (column, batch), and injection method (NH_3, d-DIHEN) are presented for comparison.

Sample type	Name	δ^{11}B	(2SD)	n	Cleaning	Separation	Injection
Giant clam	JCt-1	17.50	0.69	6	Ox	batch	d-DIHEN
Giant clam	JCt-1	16.90	0.30	6	Ox	batch	NH_3
Giant clam	JCt-1	16.34	0.64	2	Ox	column	NH_3
Giant clam	JCt-1	16.24	0.42	2	U	batch	NH_3
Porites coral	JCp-1	24.52	0.34	6	Ox	column	NH_3
Porites coral	JCp-1	24.30	0.16	10	Ox	batch	d-DIHEN
Porites coral	JCp-1	24.65	0.60	6	Ox	batch	NH_3
Porites coral	JCp-1	24.44	0.56	6	U	column	NH_3
Porites coral	JCp-1	24.41	0.30	6	U	batch	NH_3
Porites coral	JCp-1	24.36	0.51	2	Ox	column	NH_3
Porites coral	JCp-1	24.24	0.38	2	Ox	batch	NH_3
Porites coral	NEP-1	26.56	0.34	2	U	batch	NH_3
Porites coral	NEP-1	25.51	0.38	2	Ox	column	NH_3
Porites coral	NEP-1	25.34	0.78	2	Ox	batch	NH_3
Porites coral	NEP-1	25.52	0.46	2	U	column	NH_3
Porites coral	NEP-1	25.92	0.12	2	U	batch	NH_3
Porites coral	NEP-1	25.96	0.30	2	Ox	batch	NH_3
Temperate coral	OCU-9	24.04	na	1	Ox	batch	NH_3
Temperate coral	OCU-10	23.98	na	1	Ox	batch	NH_3
Temperate coral	OCU-11	24.34	na	1	Ox	batch	NH_3
Coralline alga	JR-19	39.94	0.12	2	Ox	batch	NH_3
Coralline alga	JR-20	32.65	0.46	2	Ox	batch	NH_3
Coralline alga	JR-20	32.68	0.22	2	Ox	column	NH_3
Coralline alga	JR-21	35.07	na	1	Ox	batch	NH_3
Tropical urchin	JR-56	19.00	0.36	2	Ox	batch	NH_3
Tropical urchin	JR-57	18.64	0.11	2	Ox	batch	NH_3
Tropical urchin	JR-58	18.49	0.09	2	Ox	batch	NH_3
Temperate urchin	JR-64	14.96	0.10	2	Ox	column	NH_3
Temperate urchin	JR-64	17.60	0.80	2	Ox	batch	d-DIHEN
Temperate urchin	JR-65	17.11	1.10	2	Ox	batch	NH_3
Temperate urchin	JR-66	15.43	0.11	2	Ox	batch	NH_3
Serpulid worm tube	JR-1	19.44	na	1	Ox	batch	NH_3
Serpulid worm tube	JR-2	19.13	na	1	Ox	batch	NH_3
Serpulid worm tube	JR-3	19.21	na	1	Ox	batch	NH_3
American oyster	JR125	16.18	0.16	2	Ox	column	NH_3
American oyster	JR125	15.90	0.60	2	Ox	batch	d-DIHEN
American oyster	JR125	16.00	0.32	2	U	batch	NH_3

surements at Ifremer (Plouzané, France), including comparisons of different techniques for sample preparation and for sample introduction to the mass spectrometer. For each of the samples evaluated, neither cleaning protocol, nor method of sample preparation, nor injection system was found to cause a significant (p-value < 0.05) difference in the $\delta^{11}B_{CaCO_3}$ composition of the samples (Table 3). The most effective method for minimizing memory effects in the MC-ICPMS analyses was found to be d-DIHEN (Louvat et al., 2011). However, d-DIHEN has a complicated set-up and often generates capillary blockages arising from the aspiration of particles (e.g., resin) and/or from plasma extinction resulting from air bubble introduction. In short, sample analysis via d-DIHEN requires nearly continuous use to maintain its sta-

Table 4. Summary of the average and standard deviation (SD) of δ^{11}B for each species (‰), calculated pH of calcifying fluid (pH_{CF}), pH of seawater (pH_{SW}) during the experimental conditions, difference between pH_{CF} and pH_{SW} (ΔpH), calcification response to ocean acidification experiments (OA response; Ries et al., 2009), and shell/skeletal mineralogy (HMC: high-Mg calcite; LMC: low-Mg calcite; Ries et al., 2009). In most cases three biological replicates of each species were analyzed. NA: not available because only one biological replicate has been analyzed.

Sample type	Scientific name	δ^{11}B (SD)	pH_{CF}	pH_{SW}	ΔpH	OA response	Mineralogy
Coralline alga	*Neogoniolithion* sp.	35.89 (3.71)	9.4	8.1	1.3	Parabolic	HMC
Temperate coral	*Oculina arbuscula*	24.12 (0.19)	8.5	8.1	0.4	Threshold	Aragonite
Tropical urchin	*Eucidaris tribuloides*	18.71 (0.26)	8.1	8.0	0.1	Threshold	HMC
Serpulid worm	*Hydroides crucigera*	19.26 (0.16)	8.2	8.1	0.1	Negative	Aragonite + HMC
Temperate urchin	*Arbacia punctulata*	16.28 (0.86)	7.9	8.0	−0.1	Parabolic	HMC
American oyster	*Crassostrea virginica*	16.03 (NA)	7.9	8.2	−0.3	Negative	LMC

Note: SD is calculated from measurements of different individuals of the same species, thereby reflecting interspecimen variability. Variability arising from intra-specimen variation (i.e., variability within a single specimen) and analytical error is presented in Table 3.

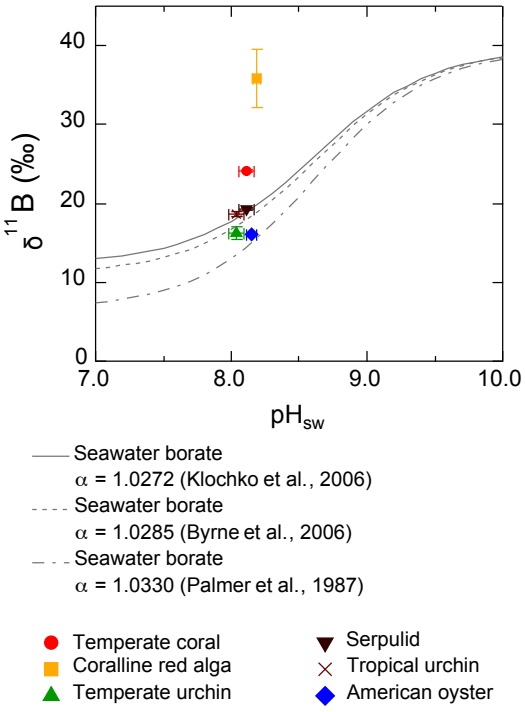

Figure 4. Boron isotopic composition (±SD) of different species of marine calcifiers as a function of seawater pH (±SD). The six species shown in this figure were grown under controlled pCO_2 conditions of ca. 409 ppm. Grey lines are theoretical seawater $\delta^{11}B_{B(OH)_4^-}$–pH curves based on different α that have been used to describe boron isotope fractionation between borate ion and boric acid in seawater (using pK_B of 8.6152 at 25 °C and 32 psu). Although $\alpha = 1.0272$ (Klochko et al., 2006) is presently the most commonly used α, $\delta^{11}B_{B(OH)_4^-}$–pH curves calculated from other values of α are also shown for comparison.

bility. In contrast, the ammonia-addition method (Al-Ammar et al., 1999, 2000) requires continuous attention by personnel while in use, due to the use of ammonia gas, but is set up and disassembled with relative ease between uses. A constant ammonia flow of 3 mL min^{-1} was necessary to maintain a sufficiently high pH to enable a fast rinse. Less than a 3 % boron memory effect was stable after 2 min, enabling a signal correction for the next sample. Both the column and batch methods of B separation yielded low blanks when < 60 µL of resin was used (see Sect. 2.5 and 2.6). However, the batch method was identified as preferable over the column chemistry method since the batch method has a lower risk of B contamination due to reduced contact time with air and the small volumes of both resin and acids (both potential sources of contamination) used in the separation process.

4.2 The $\delta^{11}B_{CaCO_3}$ compositions of a diverse range of marine calcifiers

The six species investigated exhibited a broad spectrum of $\delta^{11}B_{CaCO_3}$ compositions, ranging from 16.03 to 35.89 ‰ (Table 4) despite exposure of all species to an approximately equivalent pH_{SW} of 8 (see Table 4). Because $\delta^{11}B_{B(OH)_4^-}$ at the species' sites of calcification cannot be measured or calculated from the data at hand, it cannot be directly compared with the measured $\delta^{11}B_{CaCO_3}$ to determine if $\delta^{11}B_{CaCO_3}$ necessarily reflects calcifying fluid $\delta^{11}B_{B(OH)_4^-}$ and, thus, pH_{CF}. Assuming that only the borate ion is incorporated into biogenic $CaCO_3$ (i.e., $\delta^{11}B_{CaCO_3}$ = calcifying fluid $\delta^{11}B_{B(OH)_4}$), the wide variation in $\delta^{11}B_{CaCO_3}$ (ca. 20 ‰) amongst the investigated species reared under equivalent thermochemical conditions may indeed arise from inherent differences in pH_{CF} amongst the species. If this is the case, then the observed range in $\delta^{11}B_{CaCO_3}$ amongst the species (16.03 to 35.89 ‰) translates to an approximate range in pH_{CF} of 7.9–9.4.

The amount of boron (i.e., B / Ca) co-precipitated with inorganic (i.e., abiogenic) $CaCO_3$ is known to be dependent on solution pH and inorganic $CaCO_3$ precipitation rate. However, the relative abundances of the inorganic B species in solution that are incorporated into inorganic $CaCO_3$ (borate ion

and boric acid) have been shown to be independent of parent solution pH (Mavromatis et al., 2015). Although Mavromatis et al. (2015) also found that polymorph mineralogy influences both the B : Ca ratio (higher in aragonite than calcite) and coordination of B in inorganic $CaCO_3$ (tetrahedral / trigonal ratio higher in aragonite than in calcite), the B : Ca ratio alone does not appear to influence boron isotope fractionation in $CaCO_3$ (Noireaux et al., 2015). It should also be noted that these experiments (Mavromatis et al., 2015; Noireaux et al., 2015) analyzed carbonates precipitated from non-seawater solutions; therefore, further work is needed to determine the applicability of these findings to marine carbonates. Furthermore, because the borate / boric acid ratio is higher in aragonite than in calcite, aragonite-producing species (corals, serpulid worms) should have a universally lower $\delta^{11}B_{CaCO_3}$ composition than calcite-producing species (urchins, coralline algae, oysters) if shell mineralogy was the primary driver of the observed interspecific variation in $\delta^{11}B_{CaCO_3}$ compositions – a trend that is not observed (Fig. 4). Thus, interspecific differences in polymorph mineralogy cannot, alone, explain the species' disparate $\delta^{11}B_{CaCO_3}$ compositions. The more parsimonious explanation for these observed differences in $\delta^{11}B_{CaCO_3}$ appears to be differences in pH_{CF}, which would change the speciation of dissolved B at the site of calcification and therefore the isotopic composition of the borate ion that is preferentially incorporated into the organisms' $CaCO_3$.

Significant deviations from equilibrium exist in the stable isotopic compositions (e.g., O, C, B) of biogenic marine $CaCO_3$ (e.g., Hemming and Hanson, 1992; McConnaughey, 1989). Notably, many marine calcifiers exhibit $\delta^{11}B_{CaCO_3}$ that differs from the $\delta^{11}B_{B(OH)_4^-}$ of their surrounding seawater (Figs. 3 and 5). When interpreted in the context of the framework that skeletal δ^{11}B reflects pH_{CF} rather than the organism's ambient pH_{SW}, these results suggest that marine calcifiers are precipitating their $CaCO_2$ from a discrete fluid with a pH_{CF} higher than, equal to, or, for some species, below that of seawater. A second hypothesis is that pH_{CF} exerts some control over $\delta^{11}B_{B(OH)_4^-}$ at the site of calcification and, hence, $\delta^{11}B_{CaCO_3}$, but that there are other species-specific effects that also influence $\delta^{11}B_{CaCO_3}$ composition. The compatibility of these two hypotheses with existing models of biomineralization and observed $\delta^{11}B_{CaCO_3}$ for the various marine calcifiers investigated in the present study are discussed below.

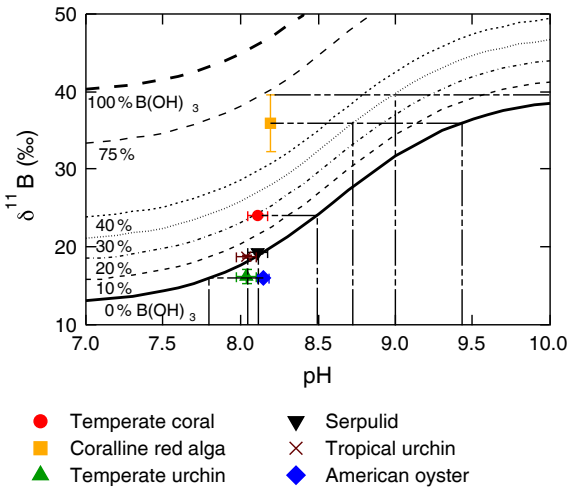

Figure 5. Exploring the potential influence of pH and boron speciation on $\delta^{11}B_{CaCO_3}$ (adapted from Rollion-Bard et al., 2011b). The solid and dashed curves represent the $\delta^{11}B_{CaCO_3}$ that would result from the incorporation of different amounts of $B(OH)_3$ into the biogenic carbonates. The dashed vertical lines represent the calculated pH_{CF} based on the assumptions that 0 % $B(OH)_3$ is incorporated into the temperate coral skeleton, American oyster shell, and temperate urchin spicule and that 0 and 30 % $B(OH)_3$ are incorporated into the coralline algal skeleton. Of all species examined, only the coralline algae has a $\delta^{11}B_{CaCO_3}$ composition that could conceivably originate at least in part from $B(OH)_3$ incorporation, although this would require a much higher level (ca. 3-fold) of skeletal $B(OH)_3$ incorporation than has been previously observed (e.g., Cusack et al., 2015; see text for more details). However, there is no clear evidence of $B(OH)_3$ incorporation based on studies of biogenic or synthetic aragonite (see text for details).

4.2.1 Coralline red alga (*Neogoniolithon* sp.)

Coralline red algae precipitate primarily high-Mg calcite from a calcifying fluid bounded by adjacent cells (Simkiss and Wilbur, 1989). Thus, biomineralization by coralline red algae occurs extracellularly but primarily within a chemically controlled environment within and adjacent to cell walls, with calcite crystals exhibiting preferred orientations – atypical of calcifying macroalgae (Simkiss and Wilbur, 1989). The average $\delta^{11}B_{CaCO_3}$ for the branching, non-articulated coralline red alga *Neogoniolithion* sp. evaluated in this study (35.89 ± 3.71 ‰; $n = 3$; Tables 3 and 4) is higher than the $\delta^{11}B_{CaCO_3}$ composition of any other calcifying marine organism evaluated to date (Table 5). Of particular interest, one of the coralline red alga specimens evaluated in this study exhibited $\delta^{11}B_{CaCO_3}$ (39.94 ‰, Table 3) similar to the average δ^{11}B of the total dissolved boron in seawater (i.e., comprising the δ^{11}B composition of both dissolved borate and boric acid; 39.61 ‰) determined by Foster et al. (2010), raising the possibility that coralline red algae incorporate both species of dissolved inorganic boron during calcification. In support of this argument, Cusack et al. (2015) provide NMR data indicating that 30 % of the B incorporated into the coralline red alga *Lithothamnion glaciale* was present as boric acid. However, since the coralline red algae were reared at a pH_{SW} of 8.1, the $\delta^{11}B_{CaCO_3}$ compositions observed for the coralline algae in the present study would require incorporation of both inorganic species of boron at $[B(OH)_3] : [B(OH)_4^-]$ ratios of ca. 3 : 1, which is not consistent with prior observa-

Table 5. Previously published δ^{11}B analyses of biogenic marine carbonates and seawater samples.

Sample	Mineralogy	δ^{11}B range (‰)	Reference
Modern coral	Aragonite	26.7–31.9	Vengosh et al. (1991)
Modern coral	Aragonite	23.0–24.7	Hemming and Hanson (1992)
Modern coral	Aragonite	23.5–27.0	Gaillardet and Allègre (1995)
Modern coral	Aragonite	23.9–26.2	Hemming et al. (1998)
Modern coral	Aragonite	25.2	Allison and Finch (2010)
Modern coral	Aragonite	23.56–27.88	Anagnostou et al. (2012)
Modern coral	Aragonite	21.5–28.0	Dishon et al. (2015)
Modern coral	Aragonite	21.76–23.19	Dissard et al. (2012)
Deep sea coral	Calcitic	13.7–17.3	Farmer et al. (2015)
Modern coral	Aragonite	18.52–23.96	Holcomb et al. (2014)
Modern coral	Aragonite	21.1–24.9	Hönisch et al. (2004)
Modern coral	Aragonite	23.2–28.7	McCulloch et al. (2012)
Deep sea coral	Calcitic	15.5	McCulloch et al. (2012)
Modern coral	Aragonite	22.5–24.0	Reynaud et al. (2004)
Modern coral	Aragonite	31.1–35.7	Rollion-Bard et al. (2011a)
Modern coral	Aragonite	18.6–30.6	Rollion-Bard et al. (2011b)
Modern coral	Aragonite	21–24.5	Schoepf et al. (2014)
Modern coral	Aragonite	23.6–25.2	D'Olivo et al. (2015)
Ancient coral	Aragonite	23.6–27.1	Douville et al. (2010)
Ancient coral	Aragonite	24.5–27.1	Kubota et al. (2014)
Ancient coral	Aragonite	22.5–25.5	Liu et al. (2009)
Modern coral	Aragonite	21.1–25.4	Wei et al. (2009)
Planktonic foraminifera	Calcite	14.2–19.8	Vengosh et al. (1991)
Planktonic foraminifera	Calcite	22.0–23.3	Sanyal et al. (1995)
Planktonic foraminifera	Calcite	18.4	Sanyal et al. (1997)
Benthic foraminifera	Calcite	13.3, 20.3, 32.0	Vengosh et al. (1991)
Benthic foraminifera	Calcite	20.5, 21.4	Sanyal et al. (1995)
Bulk foraminifera	Calcite	10.5, 11.5, 14.8, 16.2, 17.0	Spivak et al. (1993)
Planktonic foraminifera	Calcite	17.1, 22.9	Kasemann et al. (2009)
Planktonic foraminifera	Calcite	20.6–25.4	Ni et al. (2007)
Benthic foraminifera	Calcite	14.5–16.8	Rae et al. (2011)
Benthic foraminifera	Calcite	18–30.1	Rollion-Bard and Erez (2010)
Benthic foraminifera	Calcite	15.8–17.4	Yu et al. (2010)
Planktonic foraminifera	Calcite	16.9–17.9	Yu et al. (2013)
Planktonic foraminifera	Calcite	19.1–22.2	Bartoli et al. (2011)
Planktonic foraminifera	Calcite	16.2–19.8	Foster (2008)
Planktonic foraminifera	Calcite	15.2–17.2	Foster et al. (2012)
Benthic foraminifera	Calcite	13.09–13.37	Foster et al. (2012)
Planktonic foraminifera	Calcite	18.9–21.8	Foster and Sexton (2014)
Planktonic foraminifera	Calcite	20.8–23.3	Hönisch and Hemming (2005)
Planktonic foraminifera	Calcite	21.7–23.4	Hönisch et al. (2009)
Benthic foraminifera	Calcite	18.0	Kaczmarek et al. (2015)
Planktonic foraminifera	Calcite	15.1–16.4, 18.9–21.4	Martínez-Botí et al. (2015a)
Planktonic foraminifera	Calcite	19.1–19.8, 19.4–20.8	Martínez-Botí et al. (2015b)
Planktonic foraminifera	Calcite	24.2–25.7	Palmer et al. (2010)
Mixed foraminifera	Calcite	19.4–27.7	Palmer (1998)
Mixed foraminifera	Calcite	20.8–26.6	Pearson and Palmer (1999)
Planktonic foraminifera	Calcite	11–13.5, 21.6–25.5	Pearson and Palmer (2000)
Benthic foraminifera	Calcite	15.2–16.2	Rae et al. (2014)
Planktonic foraminifera	Calcite	13.6–15.8	Penman and Hönisch (2014)
Echinoid	High-Mg calcite	22.7–22.9	Hemming and Hanson (1992)
Goniolithon	High-Mg calcite	22.4	Hemming and Hanson (1992)
Encrusting red algae	High-Mg calcite	23.0	Hemming and Hanson (1992)
Thecidellina	Calcite	21.5–22.5	Hemming and Hanson (1992)
Other carbonates	Aragonite	19.1–24.8	Hemming and Hanson (1992)
Seawater	Seawater	39.9–40.2	Hemming and Hanson (1992)
Seawater	Seawater	37.7–40.4	Foster et al. (2010)

tions for inorganic and biogenic calcite. For example, Cusack et al. (2015) reported 30 % trigonal boron in the calcite lattice of a different species of coralline alga. Therefore, boric acid incorporation alone cannot explain the anomalously elevated $\delta^{11}B_{CaCO_3}$ observed here for coralline algae (see also discussion in Donald et al., 2017). Moreover, although nuclear magnetic resonance spectroscopy reveals that trigonal boron is present in the calcite lattice, it cannot determine whether boric acid was incorporated directly into the calcite lattice, or if the trigonal boron originated from borate post-mineralization (e.g., see alternative mechanisms of boron incorporation discussed in Klochko, 2006; Noireaux et al., 2015). Nevertheless, if 30 % of the B in the calcite lattice of coralline algal skeleton is indeed incorporated directly as trigonal boron, as reported by Cusack et al. (2015), pH_{CF} would still need to be as high as 9 to explain the anomalously high $\delta^{11}B_{CaCO_3}$ observed for some specimens (see Fig. 5). Short et al. (2015) observed that epiphytic turf algae can increase pH_{SW} up to 9 within their diffusive boundary layer, driven by the algae's photosynthetic drawdown of aqueous CO_2, lending further support to the idea that other types of algae, such as coralline red algae, could maintain their calcifying fluid at or above pH 9. Thus, $\delta^{11}B_{CaCO_3}$ compositions of coralline red algae may indeed reflect substantially elevated pH_{CF} (9.4; Table 4, Fig. 4), suggesting that coralline red algae are highly efficient at removing protons and/or dissolved inorganic carbon from their calcifying medium.

4.2.2 Temperate coral (*O. arbuscula*)

The average $\delta^{11}B_{CaCO_3}$ for the temperate coral *O. arbuscula* evaluated in this study (24.12 ± 0.19 ‰; $n = 3$; Tables 3 and 4) is consistent with previously published values for aragonitic corals (Table 5; see references therein). Generally, aragonitic corals are enriched in ^{11}B when compared with a theoretical borate δ^{11}B–pH curve (see Figs. 2 and 4). The main vital effect typically used to explain ^{11}B enrichment in corals, relative to seawater, is an increase in pH at the coral's site of calcification (e.g., Anagnostou et al., 2012; McCulloch et al., 2012; Rollion-Bard et al., 2011b; Trotter et al., 2011; Wall et al., 2016). This hypothesis is supported by in situ measurements of pH using microelectrodes (e.g., Al-Horani et al., 2003; Ries, 2011) and pH-sensitive fluorescent dyes (Venn et al., 2009, 2011, 2013). The δ^{11}B of the coral's skeleton is consistent with incorporation of less than 30 % of boric acid into the coral's aragonite lattice. Given that independent techniques (pH microelectrode, pH-sensitive dye) suggest that corals elevate their calcifying fluid pH within the range estimated from coral skeletal δ^{11}B using established δ^{11}B–pH relationships, and that there have been no direct measurements to date of trigonal boron in coral's aragonite skeleton, we interpret δ^{11}B results for these temperate coral skeletons to be consistent with the assertion that coral skeletal δ^{11}B is controlled primarily by coral calcifying fluid pH.

4.2.3 Tropical and temperate urchins (*E. tribuloides*, *A. punctulata*)

The average $\delta^{11}B_{CaCO_3}$ values for the tropical urchin *E. tribuloides* (18.71 ± 0.26 ‰; $n = 3$; Tables 3 and 4) and the temperate urchin *A. punctulata* (16.28 ± 0.86 ‰; $n = 3$; Tables 3 and 4) evaluated in this study, which were both reared at equivalent seawater conditions ($pH_{SW} = 8.0$; 25 °C; 32 psu; Table 4), are lower than $\delta^{11}B_{CaCO_3}$ previously reported for other echinoid species (see Table 4; 22.7–22.8 ‰) but are close to theoretical values of dissolved borate at the same pH_{SW} (17.33 ‰; Fig. 4). Microelectrode evidence and pH-sensitive dye suggest that urchins calcify from fluids with a pH_{CF} and composition similar to that of seawater (Stumpp et al., 2012), which is supported by our observation that urchin $\delta^{11}B_{CaCO_3}$ is similar to δ^{11}B of dissolved borate. The difference between the $\delta^{11}B_{CaCO_3}$ of these two species of urchin and the theoretical value of δ^{11}B for seawater borate (17.33 ‰) is +1.38 ‰ for the tropical urchin and −1.05 ‰ for the temperate urchin – a difference that exceeds their inter-specimen variability (±0.26 ‰ for the tropical urchin; ±0.86 ‰ for the temperate urchin, determined as standard deviation; see Table 5). However, this deviation in $\delta^{11}B_{CaCO_3}$ could arise from differences in the pH of their calcifying environment of only ± 0.1 units (e.g., pH_{CF} of 8.1 and 7.9 yield δ^{11}B of calcification site borate of 18.4 and 16.4 ‰, respectively; see Table 4). Thus, if deviations in urchin $\delta^{11}B_{CaCO_3}$ from seawater borate δ^{11}B indeed reflect urchins' ability to modify pH at their site of calcification, these modifications appear to be relatively minor (i.e., ± 0.1 pH units) and not always in a direction that favours calcification – consistent with Stumpp et al.'s (2012) observation that urchin biomineralization can occur in cellular compartments where pH_{CF} is lower than that of seawater. The relatively low δ^{11}B of the urchins' tests is not consistent with the hypothesis that significant boric acid is incorporated into the urchins' high-Mg calcite lattice (Fig. 5).

4.2.4 Serpulid worm tube (*H. crucigera*)

The average $\delta^{11}B_{CaCO_3}$ for the calcareous tube of the serpulid worm *H. crucigera* evaluated in this study (19.26 ± 0.16 ‰; $n = 3$; Tables 3 and 4) is close to the theoretical value of δ^{11}B for seawater borate (Fig. 4). The serpulid worm *H. crucigera* produces its calcareous tube from a combination of aragonite and high-Mg calcite (Ries, 2011b). The worm initially produces a slurry of $CaCO_3$ granules in a pair of anterior glands, which ultimately coalesces within a matrix of inorganic and organic components (Hedley, 1956). The samples of *H. crucigera* evaluated in this study were exposed to environmental conditions ($pH_{SW} = 8.1$; 25 °C; 32 psu; Table 4) yielding a theoretical seawater $\delta^{11}B_{B(OH)_4^-}$ of 18.38 ‰, which is 0.88 ‰ less than $\delta^{11}B_{CaCO_3}$ measured for this species. Similar to the tropical urchin discussed above, the serpulid worm could generate this divergence in

$\delta^{11}B_{CaCO_3}$ from seawater $\delta^{11}B_{B(OH)_4^-}$ by elevating pH_{CF} by 0.08 units relative to pH_{SW}. The relatively low δ^{11}B of the serpulid worm tube is not consistent with significant boric acid incorporation into the worm's calcite and aragonite lattices (Fig. 5). It should be noted that by producing their tubes from a mixture of aragonite and HMC, serpulid worm biomineralization and the resulting $CaCO_3$ matrix is fundamentally different those that of the other marine calcifiers evaluated in this study, which are predominantly monomineralic. To our knowledge, these are the first reported B isotope measurements for serpulid worm tubes and the δ^{11}B values for this mixed mineralogy precipitating organism are not consistent with significant boric acid incorporation into the carbonate lattice (Fig. 5).

4.2.5 American oyster (*C. virginica*)

The $\delta^{11}B_{CaCO_3}$ for the American oyster *C. virginica* evaluated in this study (16.03 ‰; $n = 1$; Tables 3 and 4) is less than the theoretical value of seawater $\delta^{11}B_{B(OH)_4^-}$ at equivalent pH_{SW} (Fig. 4). Oysters construct their shells of LMC (aragonite during the larval stage) from a discrete calcifying fluid known as the extrapallial fluid (e.g., Crenshaw, 1972), with hemocytes and organic templates playing a potentially important role in crystal nucleation (e.g., Marie et al., 2012; Mount et al., 2004; Weiner et al., 1984; Wheeler, 1992; Wilbur and Saleuddin, 1983). The specimens of *C. virginica* evaluated in this study were grown in seawater conditions ($pH_{SW} = 8.2$; 25 °C; 32 psu; Table 4) that yield a theoretical seawater $\delta^{11}B_{B(OH)_4^-}$ of 19.57 ‰, which is 3.54 ‰ greater than $\delta^{11}B_{CaCO_3}$ measured for this species. The observation that oyster $\delta^{11}B_{CaCO_3}$ is substantially less than seawater $\delta^{11}B_{B(OH)_4^-}$ suggests that the pH_{CF} of oyster extrapallial fluid is less than the pH of the oyster's surrounding seawater. Indeed, pH microelectrode measurements show that the pH of oyster EPF (pH_{EPF}) is approximately 0.5 units less than seawater pH, which has been attributed to metabolically driven accumulation of dissolved CO_2 when the oyster's shell is closed (Crenshaw, 1972; Littlewood and Young, 1994; Michaelidis et al., 2005). Oysters appear to overcome the low $CaCO_3$ saturation state in the EPF, compared to corals that maintain an elevated $CaCO_3$ saturation state at their site of calcification, by using organic templates to facilitate biomineral growth (e.g., Addadi et al., 2003; Marie et al., 2012; Weiner et al., 1984) and/or maintaining elevated levels of dissolved inorganic carbon within the EPF. The oyster could generate this negative divergence in $\delta^{11}B_{CaCO_3}$ from seawater borate δ^{11}B by decreasing pH_{CF} by 0.35 units (Table 4), which, given the proximity of the independent pH microelectrode measurements of oyster EPF (0.5 units less than seawater pH; Crenshaw, 1972), seems to be a plausible explanation for why oyster $\delta^{11}B_{CaCO_3}$ falls below the theoretical seawater $\delta^{11}B_{B(OH)_4^-}$–pH curve (Klochko et al., 2009; Fig. 5). The relatively low δ^{11}B of the oyster calcite is not consistent with significant boric acid incorporation into the oyster's calcite lattice (Fig. 5). To the authors' knowledge, these are the first B isotope analyses reported for oysters.

4.3 Estimating pH_{CF} from $\delta^{11}B_{CaCO_3}$

The six species of calcifying marine organisms investigated in the present study exhibited average $\delta^{11}B_{CaCO_3}$ ranging from 16.27 to 35.09 ‰ (Table 3). Given that all six species were grown under nearly equivalent controlled laboratory conditions, the large interspecific range in $\delta^{11}B_{CaCO_3}$ supports the hypothesis that $\delta^{11}B_{CaCO_3}$ of biogenic carbonates is not simply inherited from $\delta^{11}B_{B(OH)_4^-}$ of the organism's surrounding seawater (see Table 5 and references therein). Rather, we assert that this species-dependent variability in $\delta^{11}B_{CaCO_3}$ is driven by interspecific differences in the organisms' pH_{CF}. To explore this assertion, $\delta^{11}B_{CaCO_3}$ values were converted to pH_{CF} from measured seawater temperature, salinity, a total dissolved boron δ^{11}B value of 39.61 ± 0.20 ‰ (Foster et al., 2010), and an α of 1.0272 (Klochko et al., 2006; Table 4). In the absence of direct measurements of calcifying fluid temperature, salinity, and total dissolved boron δ^{11}B, these parameters are assumed to be equivalent to those of the organism's surrounding seawater. Assuming that only borate is incorporated into the organisms' shells and skeletons (see Table 4), these calculations yield a pH_{CF} (in order of decreasing magnitude) of 9.4 for the coralline red alga (*Neogoniolithion* sp.), 8.5 for the temperate coral (*O. arbuscula*), 8.2 for the serpulid worm (*H. crucigera*), 8.1 for the tropical urchin *(E. tribuloides*), and 7.9 for the temperate urchin (*A. punctulata*) and American oyster (*C. virginica*).

4.3.1 Nonlinearity of the $\delta^{11}B_{CaCO_3}$–pH_{CF} relationship relative to pK_B

The determination of pH_{CF} from pK_B, total boron δ^{11}B of calcifying fluid ($\delta^{11}B_{CF}$), and $\delta^{11}B_{CaCO_3}$ can be summarized with the following equation:

$$pH_{CF} = pK_B - \log\left(\frac{\delta^{11}B_{CaCO_3} - \delta^{11}B_{CF}}{\delta^{11}B_{CF} - \left(\alpha \times \delta^{11}B_{CaCO_3}\right) - 1000(\alpha - 1)}\right),$$

where pK_B is 8.6152 (at 25 °C and 32 psu; Dickson, 1990), $\delta^{11}B_{CF}$ is 39.61 ‰ (inherited from $\delta^{11}B_{SW}$; Foster et al., 2010), and α is 1.0272 (Klochko et al., 2006).

The sensitivity of $\delta^{11}B_{CaCO_3}$ to changes in pH_{CF} increases as pH_{CF} approaches pK_B (8.6152; Table S1). For example, a change in pH_{CF} from 7.75 to 7.80 predicts a $\delta^{11}B_{CaCO_3}$ difference of 0.35 ‰ (15.77–15.42 ‰), whereas a change in pH from 8.35 to 8.40 predicts a $\delta^{11}B_{CaCO_3}$ difference of 0.74 ‰ (22.59–21.85 ‰). Thus, the relationship between pH_{CF} and $\delta^{11}B_{CaCO_3}$ is nonlinear over the pH_{CF} range of interest ($7 < pH < 10$), with pH having the greatest influence on $\delta^{11}B_{CaCO_3}$ as pH_{CF} approaches pK_B.

Fortuitously, the calcifiers investigated in the present study maintain their pH_{CF} within approximately 1 pH unit of pK_B

(i.e., over the interval where small differences in pH_{CF} cause relatively large differences in $\delta^{11}B_{CaCO_3}$). Therefore, for these organisms, it will be easier to obtain precise measurements of expected differences in $\delta^{11}B_{CaCO_3}$ and, thus, differences in pH_{CF}. Conversely, it will be harder to obtain precise measurements of the differences in $\delta^{11}B_{CaCO_3}$ (and therefore pH_{CF}) for calcifiers that maintain their pH_{CF} more distal from pK_B – if such calcifiers indeed exist.

Along these same lines, slight differences in pH_{SW} of the experimental treatments (also proximal to pK_B) could conceivably translate to relatively large changes in $\delta^{11}B_{B(OH)_4^-}$ amongst the species' seawater treatments and, thus, their calcifying fluid $\delta^{11}B_{B(OH)_4^-}$ and $\delta^{11}B_{CaCO_3}$. However, the small range of pH_{SW} for the different species' experimental treatments (8.0–8.2; Table 4) could only account for a 2.24 ‰ range in $\delta^{11}B_{CaCO_3}$ (Table S1), which is far less than the ca. 20 ‰ range that was observed amongst the different species in the present study. It therefore follows that the large variability in $\delta^{11}B_{CaCO_3}$ (ca. 20 ‰) observed for the investigated species requires an alternative explanation, such as species-level differences in their pH_{CF}.

4.3.2 Sensitivity of δ^{11}B-derived pH_{CF} to choice of α

As discussed in the introduction (Sect. 1.1), much work has gone into establishing an α that accurately describes the pH-dependent relationship between δ^{11}B of dissolved borate and boric acid in seawater (see Xiao et al., 2014, for detailed discussion), with the earliest published paleo-pH reconstructions using a theoretical value of 1.0194 (Kakihana et al., 1977; see Fig. 2). An empirical α of 1.0272 (Klochko et al., 2006) has now been shown to better predict $\delta^{11}B_{B(OH)_4^-}$, viz. $\delta^{11}B_{CaCO_3}$, across the range of pH relevant for seawater (Rollion-Bard and Erez, 2010; Xiao et al., 2014). However, $\delta^{11}B_{CaCO_3}$ values of many species of calcifying marine organisms fall either above or below theoretical $\delta^{11}B_{B(OH)_4^-}$–pH_{SW} curves. It has long been suggested (and shown for corals) that calcifying organisms diverge from the predicted $\delta^{11}B_{CaCO_3}$ due to their ability to modify the pH of their calcifying environments (e.g., Anagnostou et al., 2012; Hönisch et al., 2004; Krief et al., 2010; McCulloch et al., 2012; Rae et al., 2011; Reynaud et al., 2004; Trotter et al., 2011; Wall et al., 2016). In the present study, species-specific divergences in $\delta^{11}B_{CaCO_3}$ from the theoretical $\delta^{11}B_{B(OH)_4^-}$–pH_{SW} curves are interpreted as evidence of the differing capacities of calcifying marine species to modify pH_{CF}. Importantly, existing models of biomineralization for each species are generally compatible with these $\delta^{11}B_{CaCO_3}$-derived estimates of pH_{CF} (see Sect. 4.2).

Although an α of 1.0272 (Klochko et al., 2006) was used in the present study to estimate pH_{CF}, other theoretical values for α, yielding slightly different $\delta^{11}B_{B(OH)_4^-}$–pH_{SW} curves (e.g., Byrne et al., 2006; Palmer et al., 1987; see Fig. 4), will yield slightly different estimates of pH_{CF} for each organism. For example, using α values of 1.033 (Palmer et al., 1987), 1.0285 (Byrne et al. 2006), 1.0272 (Klochko et al. 2006), and 1.0194 (Kakihana et al. 1977) and a $\delta^{11}B_{CaCO_3}$ of 24.12 ‰ (temperate coral; $pH_{SW} = 8.1$) yields pH_{CF} values of 8.7, 8.6, 8.5, and 8.1, respectively – a range of 0.6 pH units. It should also be noted that the lower the $\delta^{11}B_{CaCO_3}$, the more sensitive the reconstructed pH is to choice of α. For example, changing α from 1.0272 to 1.0330 will result in a 0.24 pH unit shift for $\delta^{11}B_{CaCO_3}$ of 20 ‰ but only a 0.12 and 0.08 pH unit shift for $\delta^{11}B_{CaCO_3}$ of 30 and 39.5 ‰, respectively (see Fig. 4). This underscores the importance of using the same α when comparing $\delta^{11}B_{CaCO_3}$-based estimate of pH_{CF} amongst species.

4.3.3 Implications of $\delta^{11}B_{CaCO_3}$-derived estimates of pH_{CF} for species-specific vulnerability to ocean acidification

Establishing how marine organisms calcify is a critical requirement for understanding and, ideally, predicting their physiological responses to future ocean acidification (e.g., Kleypas et al., 2006). Although it is widely known that many species of marine calcifiers promote calcification by raising pH at their site of calcification, the present study identifies the degree to which this strategy for biocalcification is employed across a range of divergent taxa. Marine calcifiers that employ this strategy for calcification may be more resilient to the effects of ocean acidification because their high pH_{CF} (relative to pH_{SW}) would cause HCO_3^- (elevated due to increased pCO_2) to dissociate into CO_3^{2-} for calcification, helping the organism to maintain an elevated Ω at its site of calcification (Ries et al., 2009). Evaluation of this hypothesis in the context of the results of the present study shows that, indeed, the different species' $\delta^{11}B_{CaCO_3}$ and calculated pH_{CF} exhibit a moderate, inverse relationship with their experimentally determined vulnerability to ocean acidification (Ries et al., 2009). Species exhibiting more resilient "parabolic" (e.g., coralline red alga) and "threshold" (e.g., coral, tropical urchin) responses to ocean acidification generally exhibited a higher $\delta^{11}B_{CaCO_3}$ and, thus, pH_{CF} than species exhibiting the more vulnerable "negative" responses (e.g., oyster, serpulid worm) to ocean acidification (Table 4). The temperate urchin was the exception to this general trend, as it exhibited a relatively resilient parabolic response to ocean acidification yet maintained $\delta^{11}B_{CaCO_3}$ and, thus, pH_{CF} close to that of pH_{SW}. These results support the assertion that interspecific differences in pH_{CF} contribute to marine calcifiers' differential responses to ocean acidification – highlighting the need for future queries into the mechanisms driving boron isotope fractionation, biomineralization, and vulnerability to ocean acidification of marine calcifying organisms.

5 Conclusions

This study establishes the methodology for measuring stable boron isotopes at Ifremer (Plouzané, France) and reveals that neither cleaning protocol (oxidized vs. untreated), nor method of sample preparation (batch vs. column), nor injection system (*d*-DIHEN vs. ammonia addition) causes a significant difference in the measured $\delta^{11}B_{CaCO_3}$ of the evaluated samples and standards. The batch method of boron extraction is identified as preferable to the column chemistry method because the risk of B contamination is reduced in the batch method due to shorter exposure to potential contaminants and smaller reagent volumes.

This newly established method for measuring stable boron isotopes at Ifremer was used to measure the $\delta^{11}B_{CaCO_3}$ of six species of marine calcifiers that were all grown under equivalent seawater conditions. The coralline red alga *Neogoniolithion* sp. (35.89 ± 3.71 ‰; $n = 3$) exhibited the highest $\delta^{11}B_{CaCO_3}$, followed by the temperate coral *O. arbuscula* (24.12 ± 0.19 ‰; $n = 3$), the tube of the serpulid worm *H. crucigera* (19.26 ± 0.16 ‰; $n = 3$), the tropical urchin *E. tribuloides* (18.71 ± 0.26 ‰; $n = 3$), the temperate urchin *A. punctulata* (16.28 ± 0.86 ‰; $n = 3$), and the temperate oyster *C. virginica* (16.03 ‰; $n = 1$). The observed ca. 20 ‰ range in $\delta^{11}B_{CaCO_3}$ composition of the investigated species constitutes the largest range in biogenic $\delta^{11}B_{CaCO_3}$ reported to date.

Consideration of these extreme interspecific differences in $\delta^{11}B_{CaCO_3}$ in the context of existing models of biomineralization for the investigated species, combined with published measurements of pH_{CF} for some of the species, generally supports the assertion that most marine calcifiers precipitate their $CaCO_3$ from a discrete calcifying medium with a pH that is either greater than, equivalent to, or, for some species, less than external seawater pH. Furthermore, the observation that the different species' $\delta^{11}B_{CaCO_3}$ and calculated pH_{CF} generally varied inversely with their experimentally determined vulnerability to ocean acidification suggests that a species' relative resilience (or vulnerability) to OA may be influenced by their ability (or lack thereof) to maintain an elevated pH_{CF}. These observations contribute to the growing body of work that uses $\delta^{11}B_{CaCO_3}$ as a tool to advance understanding of the mechanisms by which marine calcifiers build and maintain their shells and skeletons and, ultimately, how these organisms will respond to anthropogenic CO_2-induced ocean acidification.

Data availability. All data are published in this paper or in the Supplement: therefore all the data are publicly accessible.

The Supplement related to this article is available online at https://doi.org/10.5194/bg-15-1447-2018-supplement.

Author contributions. RAE and JBR conceived of the project and wrote the proposals that funded the work. JBR performed the culturing experiments. RAE, JNS, and JBR contributed to the experimental design. JNS, YWL, MG, EP, and RAE contributed to developing the method of boron isotope analysis. JNS performed the measurements with assistance from EP. JNS conducted the data analysis. Interpretation was led by JNS and RAE with input from JBR and YWL. JNS drafted the paper, which was edited by all authors. This is publication no. 361 from Northeastern's Marine Science Center.

Competing interests. The authors declare that they have no conflict of interest.

Acknowledgements. This work was supported by the Laboratoire d'Excellence LabexMER (ANR-10-LABX-19) and co-funded by a grant from the French government under the program Investissements d'Avenir, as well as by a grant from the Regional Council of Brittany (SAD programme). Robert A. Eagle and Justin B. Ries also acknowledge support from National Science Foundation grants OCE-1437166 and OCE-1437371. We thank Juan Pablo D'Olivo and the members of the UWA lab for supplying us with an aliquot of the NEP standard.

Edited by: Xinming Wang
Reviewed by: Jesse Farmer and two anonymous referees

References

Addadi, L., Raz, S., and Weiner, S.: Taking advantage of disorder: Amorphous calcium carbonate and its roles in biomineralization, Adv. Mater., 15, 959–970, https://doi.org/10.1002/adma.200300381, 2003.

Al-Ammar, A. S., Gupta, R. K., and Barnes, R. M.: Elimination of boron memory effect in inductively coupled plasma-mass spectrometry by ammonia gas injection into the spray chamber during analysis, Spectrochim. Acta B, 55, 629–635, https://doi.org/10.1016/S0584-8547(00)00197-X, 2000.

Al-Horani, F. A., Al-Moghrabi, S. M., and de Beer, D.: The mechanism of calcification and its relation to photosynthesis and respiration in the scleractinian coral *Galaxea fascicularis*, Mar. Biol., 142, 419–426, https://doi.org/10.1007/s00227-002-0981-8, 2003.

Allison, N. and Finch, A. A.: δ^{11}B, Sr, Mg and B in a modern Porites coral: the relationship between calcification site pH and skeletal chemistry, Geochim. Cosmochim. Ac., 74, 1790–1800, https://doi.org/10.1016/j.gca.2009.12.030, 2010.

Ameye, L., Compère, P., Dille, J., and Dubois, P.: Ultrastructure and cytochemistry of the early calcification site and of its mineralization organic matrix in *Paracentrotus lividus* (Echinodermata: Echinoidea), Histochem. Cell Biol., 110, 285–294, https://doi.org/10.1007/s004180050290, 1998.

Anagnostou, E., Huang, K.-F., You, C.-F., Sikes, E. L., and Sherrell, R. M.: Evaluation of boron isotope ratio as a pH proxy in the deep sea coral *Desmophyllum dianthus*: Evidence of physiological pH adjustment, Earth Planet. Sc. Lett., 349–350, 251–260, https://doi.org/10.1016/j.epsl.2012.07.006, 2012.

Balan, E., Pietrucci, F., Gervais, C., Blanchard, M., Schott, J., and Gaillardet, J.: First-principles study of boron speciation in calcite and aragonite, Geochim. Cosmochim. Ac., 193, 119–131, https://doi.org/10.1016/j.gca.2016.07.026, 2016.

Barker, S., Greaves, M., and Elderfield, H.: A study of cleaning procedures used for foraminiferal Mg / Ca paleothermometry, Geochem. Geophy. Geosy., 4, 1–20, https://doi.org/10.1029/2003GC000559, 2003.

Bartoli, G., Hönisch, B., and Zeebe, R. E.: Atmospheric CO_2 decline during the Pliocene intensification of Northern Hemisphere glaciations, Paleoceanography, 26, PA4213, https://doi.org/10.1029/2010PA002055, 2011.

Bates, N. R.: Interannual variability of the oceanic CO_2 sink in the subtropical gyre of the North Atlantic Ocean over the last 2 decades, J. Geophys. Res.-Ocean., 112, 1–26, https://doi.org/10.1029/2006JC003759, 2007.

Borowitzka, M. A. and Larkum, A. W. D.: Calcification in algae: Mechanisms and the role of metabolism, CRC. Crit. Rev. Plant Sci., 6, 1–45, https://doi.org/10.1080/07352688709382246, 1987.

Byrne, R. H., Yao, W., Klochko, K., Tossell, J. A., and Kaufman, A. J.: Experimental evaluation of the isotopic exchange equilibrium $^{10}B(OH)_3 + {}^{11}B(OH)_4^- = {}^{11}B(OH)_3 + {}^{10}B(OH)_4^-$ in aqueous solution, Deep-Sea Res. Pt. I, 53, 684–688, https://doi.org/10.1016/j.dsr.2006.01.005, 2006.

Byrne, R. H., Mecking, S., Feely, R. A., and Liu, X.: Direct observations of basin-wide acidification of the North Pacific Ocean, Geophys. Res. Lett., 37, 1–5, https://doi.org/10.1029/2009GL040999, 2010.

Cameron, J. N.: Post-moult calcification in the Blue Crab (Callinectes sapidus): Relationships between apparent net HC excretion, calcium and bicarbonate, J. Exp. Biol., 143, 285–304, 1989.

Catanzaro, E. J., Champion, C. E., Garner, E. L., Marinenko, G., Sappenfield, K., and Shields, W. R.: Boric acid: Isotopic and assay standard reference materials, US National Bureau of Standards, Special Publication, 260, 1–17, 1970.

Cohen, A. L. and McConnaughey, T. A.: Geochemical Perspectives on Coral Mineralization, in: Biomineralization, edited by: Dove, P. M., De Yoreo, J. J., and Weiner, S., Mineralogical Society of America Geochemical Society, 151–188, 2003.

Cohen, A. and Holcomb, M.: Why corals care about ocean acidification: Uncovering the mechanism, Oceanography, 22, 118–127, https://doi.org/10.5670/oceanog.2009.102, 2009.

Crenshaw, M. A.: The inorganic composition of molluscan extrapallial fluid, Biol. Bull., 143, 506–512, https://doi.org/10.2307/1540180, 1972.

Cuif, J. P. and Dauphin, Y.: The Environment Recording Unit in coral skeletons: a synthesis of structural and chemical evidences for a biochemically driven, stepping-growth process in fibres, Biogeosciences, 2, 61–73, https://doi.org/10.5194/bg-2-61-2005, 2005.

Cusack, M., Kamenos, N. A., Rollion-Bard, C., and Tricot, G.: Red coralline algae assessed as marine pH proxies using ^{11}B MAS NMR, Sci. Rep., 5, 8175, https://doi.org/10.1038/srep08175, 2015.

De Beer, D. and Larkum, A. W. D.: Photosynthesis and calcification in the calcifying algae *Halimeda discoidea* studied with microsensors, Plant Cell Environ., 24, 1209–1217, https://doi.org/10.1046/j.1365-3040.2001.00772.x, 2001.

Dickson, A. G.: Thermodynamics of the dissociation of boric acid in synthetic seawater from 273.15 to 318.15 K, Deep-Sea Res. Pt. A, 37, 755–766, https://doi.org/10.1016/0198-0149(90)90004-F, 1990.

Dishon, G., Fisch, J., Horn, I., Kaczmarek, K., Bijma, J., Gruber, D. F., Nir, O., Popovich, Y., and Tchernov, D.: A novel paleobleaching proxy using boron isotopes and high-resolution laser ablation to reconstruct coral bleaching events, Biogeosciences, 12, 5677–5687, https://doi.org/10.5194/bg-12-5677-2015, 2015.

Dissard, D., Douville, E., Reynaud, S., Juillet-Leclerc, A., Montagna, P., Louvat, P., and McCulloch, M.: Light and temperature effects on δ^{11}B and B : Ca ratios of the zooxanthellate coral *Acropora* sp.: results from culturing experiments, Biogeosciences, 9, 4589–4605, https://doi.org/10.5194/bg-9-4589-2012, 2012.

D'Olivo, J. P., McCulloch, M. T., Eggins, S. M., and Trotter, J.: Coral records of reef-water pH across the central Great Barrier Reef, Australia: assessing the influence of river runoff on inshore reefs, Biogeosciences, 12, 1223–1236, https://doi.org/10.5194/bg-12-1223-2015, 2015.

Donald, H. K., Ries, J. B., Stewart, J. A., Fowell, S. E., and Foster, G. L.: Boron isotope sensitivity to seawater pH change in a species of *Neogoniolithon* coralline red alga, Geochim. Cosmochim. Ac., 217, 240–253, https://doi.org/10.1016/j.gca.2017.08.021, 2017.

Doney, S. C., Fabry, V. J., Feely, R. A., and Kleypas, J. A.: Ocean Acidification: The other CO_2 problem, Annu. Rev. Mar. Sci., 1, 169–192, https://doi.org/10.1146/annurev.marine.010908.163834, 2009.

Dore, J. E., Lukas, R., Sadler, D. W., Church, M. J., and Karl, D. M.: Physical and biogeochemical modulation of ocean acidification in the central North Pacific, P. Natl. Acad. Sci. USA, 106, 12235–12240, https://doi.org/10.1073/pnas.0906044106, 2009.

Douville, E., Paterne, M., Cabioch, G., Louvat, P., Gaillardet, J., Juillet-Leclerc, A., and Ayliffe, L.: Abrupt sea surface pH change at the end of the Younger Dryas in the central sub-equatorial Pacific inferred from boron isotope abundance in corals (*Porites*), Biogeosciences, 7, 2445–2459, https://doi.org/10.5194/bg-7-2445-2010, 2010.

Fabry, V. J., Seibel, B. A., Feely, R. A., and Orr, J. C.: Impacts of ocean acidification on marine fauna and ecosystem processes, ICES J. Mar. Sci., 65, 414–432, 2008.

Farmer, J. R., Hönisch, B., Robinson, L. F., and Hill, T. M.: Effects of seawater-pH and biomineralization on the boron isotopic composition of deep-sea bamboo corals, Geochim. Cosmochim. Ac., 155, 86–106, https://doi.org/10.1016/j.gca.2015.01.018, 2015.

Feely, R. A., Sabine, C. L., Hernandez-Ayon, J. M., Ianson, D., and Hales, B.: Evidence for upwelling of corrosive "Acidified" water onto the continental shelf, Science, 13, 1490–1492, https://doi.org/10.1126/science.1155676, 2008.

Feely, R. A., Alin, S. R., Carter, B., Bednaršek, N., Hales, B., Chan, F., Hill, T. M., Gaylord, B., Sanford, E., Byrne R. H., Sabine, C. L., Greeley, D., and Juranek, L.: Chemical and biological impacts of ocean acidification along the west coast of North America, Estuar. Coast. Shelf S., 183, 260–270, https://doi.org/10.1016/j.ecss.2016.08.043, 2016.

Foster, G. L.: Seawater pH, pCO2 and [$CO3^{2-}$] variations in the Caribbean Sea over the last 130kyr: A boron isotope and B / Ca study of planktic foraminifera, Earth Planet. Sc. Lett., 271, 254–266, https://doi.org/10.1016/j.epsl.2008.04.015, 2008.

Foster, G. L., Lear, C. H., and Rae, J. W. B.: The evolution of pCO_2, ice volume and climate during the middle Miocene, Earth Planet. Sc. Lett., 341–344, 243–254, https://doi.org/10.1016/j.epsl.2012.06.007, 2012.

Foster, G. L., Hönisch, B., Paris, G., Dwyer, G. S., Rae, J. W. B., Elliott, T., Gaillardet, J., Hemming, N. G., Louvat, P., and Vengosh, A.: Interlaboratory comparison of boron isotope analyses of boric acid, seawater and marine $CaCO_3$ by MC-ICPMS and NTIMS, Chem. Geol., 358, 1–14, https://doi.org/10.1016/j.chemgeo.2013.08.027, 2013.

Foster, G. L., Pogge Von Strandmann, P. A. E., and Rae, J. W. B.: Boron and magnesium isotopic composition of seawater, Geochem. Geophy. Geosy., 11, 1–10, https://doi.org/10.1029/2010GC003201, 2010.

Foster, G. L. and Sexton, P. F.: Enhanced carbon dioxide outgassing from the eastern equatorial Atlantic during the last glacial, Geology, 42, 1003–1006, https://doi.org/10.1130/G35806.1, 2014.

Gaetani, G. A. and Cohen, A. L.: Element partitioning during precipitation of aragonite from seawater: A framework for understanding paleoproxies, Geochim. Cosmochim. Ac., 78, 4617–4634, https://doi.org/10.1016/j.gca.2006.07.008, 2006.

Gaillardet, J. and Allègre, C. J.: Boron isotopic compositions of corals: Seawater or diagenesis record?, Earth Planet. Sc. Lett., 136, 665–676, https://doi.org/10.1016/0012-821X(95)00180-K, 1995.

Goldberg, W. M.: Desmocytes in the calicoblastic epithelium of the stony coral *Mycetophyllia reesi* and their attachment to the skeleton, Tissue Cell, 33, 388–394, https://doi.org/10.1054/tice.2001.0192, 2001.

González-Dávila, M., Santana Casiano, J. M., and Machín, F.: Changes in the partial pressure of carbon dioxide in the Mauritanian-Cap Vert upwelling region between 2005 and 2012, Biogeosciences, 14, 3859–3871, https://doi.org/10.5194/bg-14-3859-2017, 2017.

Hedley, R. H.: Studies of serpulid tube formation, I. The secretion of the calcareous and organic components of the tube by *Pomatoceros triqueter*, Quarterly Journal of Microscopical Science, 97, 411–419, 1956.

Heinemann, A., Fietzke, J., Melzner, F., Böhm, F., Thomsen, J., Garbe-Schnberg, D., and Eisenhauer, A.: Conditions of *Mytilus edulis* extracellular body fluids and shell composition in a pH-treatment experiment: Acid-base status, trace elements and δ^{11}B, Geochem. Geophy. Geosy., 13, Q01005, https://doi.org/10.1029/2011GC003790, 2012.

Hemming, N. G. and Hanson, G. N.: Boron isotopic composition and concentration in modern marine carbonates, Geochim. Cosmochim. Ac., 56, 537–543, https://doi.org/10.1016/0016-7037(92)90151-8, 1992.

Hemming, N. G. and Hönisch, B.: Boron Isotopes in Marine Carbonate Sediments and the pH of the Ocean, Chap. 17, in: Developments in Marine Geology, 1, 717–734, 2007.

Hemming, N. G., Guilderson, T. P., and Fairbanks, R. G.: Seasonal variations in the boron isotopic composition of coral: A productivity signal?, Global Biogeochem. Cy., 12, 581–586, https://doi.org/10.1029/98GB02337, 1998.

Henehan, M. J., Rae, J. W. B., Foster, G. L., Erez, J., Prentice, K. C., Kucera, M., and Elliott, T.: Calibration of the boron isotope proxy in the planktonic foraminifera Globigerinoides ruber for use in palaeo-CO_2 reconstruction, Earth Planet. Sc. Lett., 364, 111–122, https://doi.org/10.1016/j.epsl.2012.12.029, 2013.

Holcomb, M., McCorkle, D. C., and Cohen, A. L.: Long-term effects of nutrient and CO_2 enrichment on the temperate coral *Astrangia poculata* (Ellis and Solander, 1786), J. Exp. Mar. Bio. Ecol., 386, 27–33, https://doi.org/10.1016/j.jembe.2010.02.007, 2010.

Holcomb, M., Venn, A. A., Tambutté, E., Tambutté, S., Allemand, D., Trotter, J., and McCulloch, M.: Coral calcifying fluid pH dictates response to ocean acidification, Sci. Rep., 4, 1–4, https://doi.org/10.1038/srep05207, 2014.

Hönisch, B. and Hemming, N. G.: Ground-truthing the boron isotope-paleo-pH proxy in planktonic foraminifera shells: Partial dissolution and shell size effects, Paleoceanography, 19, 3675–3685, https://doi.org/10.1029/2004PA001026, 2004.

Hönisch, B. and Hemming, N. G.: Surface ocean pH response to variations in pCO_2 through two full glacial cycles, Earth Planet. Sc. Lett., 236, 305–314, https://doi.org/10.1016/j.epsl.2005.04.027, 2005.

Hönisch, B., Bijma, J., Russell, A., Spero, H., Palmer, M. R., Zeebe, R. E., and Eisenhauer, A.: The influence of symbiont photosynthesis on the boron isotopic composition of foraminifera shells, Mar. Micropaleontol., 49, 87–96, https://doi.org/10.1016/S0377-8398(03)00030-6, 2003.

Hönisch, B., Hemming, N. G., Grottoli, A. G., Amat, A., Hanson, G. N., and Bijma, J.: Assessing scleractinian corals as recorders for paleo-pH: Empirical calibration and vital effects, Geochim. Cosmochim. Ac., 68, 3675–3685, https://doi.org/10.1016/j.gca.2004.03.002, 2004.

Hönisch, B., Hemming, N. G., Archer, D., Siddall, M., and McManus, J. F.: Atmospheric carbon dioxide concentration across the mid-Pleistocene transition., Science, 324, 1551–4, https://doi.org/10.1126/science.1171477, 2009.

IPCC: Climate Change 2013 – The Physical Science Basis, edited by Intergovernmental Panel on Climate Change, Cambridge University Press, Cambridge, 2014.

Jorgensen, B. B., Erez, J., Revsbech, N. P., and Cohen, Y.: Symbiotic photosynthesis in a planktonic foraminifera, *Globigerinoides sacculifer* (Brady), studied with microelectrodes, Limnol. Oceanogr., 30, 1253–1267, 1985.

Kaczmarek, K., Langer, G., Nehrke, G., Horn, I., Misra, S., Janse, M., and Bijma, J.: Boron incorporation in the foraminifer *Amphistegina lessonii* under a decoupled carbonate chemistry, Biogeosciences, 12, 1753–1763, https://doi.org/10.5194/bg-12-1753-2015, 2015.

Kakihana, H., Kotaka, M., Satoh, S., Nomura, M., and Okamoto, M.: Fundamental studies on the ion-exchange separation of boron isotopes, Bull. Chem. Soc. Jpn., 50, 158–163, https://doi.org/10.1246/bcsj.50.158, 1977.

Kasemann, S. A., Schmidt, D. N., Bijma, J., and Foster, G. L.: In situ boron isotope analysis in marine carbonates and its application for foraminifera and palaeo-pH, Chem. Geol., 260, 138–147, https://doi.org/10.1016/j.chemgeo.2008.12.015, 2009.

Kiss, E.: Ion-exchange separation and spectrophotometric determination of boron in geological materials, Anal. Chim. Acta, 211, 243–256, https://doi.org/10.1016/S0003-2670(00)83684-3, 1988.

Kleypas, J. A., Feely, R. A., Fabry, V. J., Langdon, C., Sabine, C. L., and Robbins, L. L.: Impacts of ocean acidification on coral reefs and other marine calcifiers, A guide for future research, 2006.

Klochko, K., Cody, G. D., Tossell, J. A., Dera, P., and Kaufman, A. J.: Re-evaluating boron speciation in biogenic calcite and aragonite using ^{11}B MAS NMR, Geochim. Cosmochim. Ac., 73, 1890–1900, https://doi.org/10.1016/j.gca.2009.01.002, 2009.

Klochko, K., Kaufman, A. J., Yao, W., Byrne, R. H., and Tossell, J. A.: Experimental measurement of boron isotope fractionation in seawater, Earth Planet. Sc. Lett., 248, 276–285, https://doi.org/10.1016/j.epsl.2006.05.034, 2006.

Krief, S., Hendy, E. J., Fine, M., Yam, R., Meibom, A., Foster, G. L., and Shemesh, A.: Physiological and isotopic responses of scleractinian corals to ocean acidification, Geochim. Cosmochim. Ac., 74, 4988–5001, https://doi.org/10.1016/j.gca.2010.05.023, 2010.

Kroeker, K. J., Kordas, R. L., Crim, R. N., and Singh, G. G.: Meta-analysis reveals negative yet variable effects of ocean acidification on marine organisms, Ecol. Lett., 13, 1419–1434, https://doi.org/10.1111/j.1461-0248.2010.01518.x, 2010.

Kroeker, K. J., Kordas, R. L., Crim, R., Hendriks, I. E., Ramajo, L., Singh, G. S., Duarte, C. M., and Gattuso, J. P.: Impacts of ocean acidification on marine organisms: Quantifying sensitivities and interaction with warming, Glob. Change Biol., 19, 1884–1896, https://doi.org/10.1111/gcb.12179, 2013.

Kubota, K., Yokoyama, Y., Ishikawa, T., Obrochta, S., and Suzuki, A.: Larger CO_2 source at the equatorial Pacific during the last deglaciation., Sci. Rep., 4, 5261, https://doi.org/10.1038/srep05261, 2014.

Langdon, C.: Review of experimental evidence for effects of CO_2 on calcification of reef builders, in: Proc. 9th Int. Coral Reef Sym, 1–8, available from: http://people.uncw.edu/szmanta/2006pdfs/20Globalwarmingissues/Langdon9ICRSProceedingsCO2calcification.pdf, 2002.

Lee, D. and Carpenter, S. J.: Isotopic disequilibrium in marine calcareous algae, Chem. Geol., 172, 307–329, https://doi.org/10.1016/S0009-2541(00)00258-8, 2001.

Lemarchand, D., Gaillardet, J., Lewin, É., and Allègre, C. J.: The influence of rivers on marine boron isotopes and implications for reconstructing past ocean pH, Nature, 408, 951–954, https://doi.org/10.1038/35050058, 2000.

Lemarchand, D., Gaillardet, J., Göpel, C., and Manhès, G.: An optimized procedure for boron separation and mass spectrometry analysis for river samples, Chem. Geol., 182, 323–334, https://doi.org/10.1016/S0009-2541(01)00329-1, 2002.

Littlewood, D. T. J. and Young, R. E.: The effect of air-gaping behaviour on extrapallial fluid pH in the tropical oyster *Crassostrea rhizophorae*, Comp. Biochem. Physiol. A, 107, 1–6, https://doi.org/10.1016/0300-9629(94)90264-X, 1994.

Liu, Y. and Tossell, J. A.: Ab initio molecular orbital calculations for boron isotope fractionations on boric acids and borates, Geochim. Cosmochim. Ac., 69, 3995–4006, https://doi.org/10.1016/j.gca.2005.04.009, 2005.

Liu, Y., Liu, W., Peng, Z., Xiao, Y., Wei, G., Sun, W., He, J., Liu, G., and Chou, C. L.: Instability of seawater pH in the South China Sea during the mid-late Holocene: Evidence from boron isotopic composition of corals, Geochim. Cosmochim. Ac., 73, 1264–1272, https://doi.org/10.1016/j.gca.2008.11.034, 2009.

Louvat, P., Bouchez, J., and Paris, G.: MC-ICP-MS isotope measurements with Direct Injection Nebulisation (*d*-DIHEN): Optimisation and application to boron in seawater and carbonate samples, Geostand. Geoanal. Res., 35, 75–88, https://doi.org/10.1111/j.1751-908X.2010.00057.x, 2011.

Louvat, P., Moureau, J., Paris, G., Bouchez, J., Noireaux, J., and Gaillardet, J. J. J.: A fully automated direct injection nebulizer (*d*-DIHEN) for MC-ICP-MS isotope analysis: application to boron isotope ratio measurements, J. Anal. At. Spectrom., 29, 1698–1707, https://doi.org/10.1039/C4JA00098F, 2014.

Marie, B., Joubert, C., Tayale, A., Zanella-Cleon, I., Belliard, C., Piquemal, D., Cochennec-Laureau, N., Marin, F., Gueguen, Y., and Montagnani, C.: Different secretory repertoires control the biomineralization processes of prism and nacre deposition of the pearl oyster shell, P. Natl. Acad. Sci. USA, 109, 20986–20991, https://doi.org/10.1073/pnas.1210552109, 2012.

Martin, P., Goodkin, N. F., Stewart, J. A., Foster, G. L., Sikes, E. L., White, H. K., Hennige, S., and Roberts, J. M.: Deep-sea coral δ^{13}C: A tool to reconstruct the difference between seawater pH and δ^{11}B-derived calcifying fluid pH, Geophys. Res. Lett., 43, 299–308, https://doi.org/10.1002/2015GL066494, 2016.

Martínez-Botí, M. A., Foster, G. L., Chalk, T. B., Rohling, E. J., Sexton, P. F., Lunt, D. J., Pancost, R. D., Badger, M. P. S., and Schmidt, D. N.: Plio-Pleistocene climate sensitivity evaluated using high-resolution CO_2 records, Nature, 518, 49–54, https://doi.org/10.1038/nature14145, 2015a.

Martínez-Botí, M. A., Marino, G., Foster, G. L., Ziveri, P., Henehan, M. J., Rae, J. W. B., Mortyn, P. G., and Vance, D.: Boron isotope evidence for oceanic carbon dioxide leakage during the last deglaciation, Nature, 518, 219–222, https://doi.org/10.1038/nature14155, 2015b.

McConnaughey, T.: ^{13}C and ^{18}O isotopic disequilibrium in biological carbonates: I. Patterns, Geochim. Cosmochim. Ac., 53, 151–162, https://doi.org/10.1016/0016-7037(89)90282-2, 1989.

McConnaughey, T. A. and Falk, R. H.: Calcium-proton exchange during algal calcification, Biol. Bull., 180, 185–195, https://doi.org/10.2307/1542440, 1991.

McConnaughey, T. A. and Whelan, J. F.: Calcification generates protons for nutrient and bicarbonate uptake, Earth-Sci. Rev., 42, 95–117, https://doi.org/10.1016/S0012-8252(96)00036-0, 1997.

McCulloch, M., Falter, J., Trotter, J., and Montagna, P.: Coral resilience to ocean acidification and global warming through pH up-regulation, Nature Climate Change, 2, 623–627, https://doi.org/10.1038/nclimate1473, 2012.

McCulloch, M. T., Holcomb, M., Rankenburg, K., and Trotter, J. A.: Rapid, high-precision measurements of boron isotopic compositions in marine carbonates, Rapid Commun. Mass Spectrom., 28, 2704–2712, https://doi.org/10.1002/rcm.7065, 2014.

Meibom, A., Cuif, J. P., Houlbreque, F., Mostefaoui, S., Dauphin, Y., Meibom, K. L., and Dunbar, R.: Compositional variations at ultra-structure length scales in coral skeleton, Geochim. Cosmochim. Ac., 72, 1555–1569, https://doi.org/10.1016/j.gca.2008.01.009, 2008.

Michaelidis, B., Haas, D., and Grieshaber, M. K.: Extracellular and intracellular acid base status with regard to the energy metabolism in the oyster *Crassostrea gigas* during exposure to air, Physiol. Biochem. Zool., 78, 373–383, https://doi.org/10.1086/430223, 2005.

Montagna, P., McCulloch, M., Mazzoli, C., Silenzi, S., and Odorico, R.: The non-tropical coral *Cladocora caespitosa* as the new climate archive for the Mediterranean: high-resolution (∼ weekly) trace element systematics, Quaternary Sci. Rev., 26, 441–462, https://doi.org/10.1016/j.quascirev.2006.09.008, 2007.

Mount, A. S., Wheeler, A. P., Paradkar, R. P., and Snider, D.: Hemocyte-mediated shell mineralization in the eastern oyster, Science, 304, 297–300, https://doi.org/10.1126/science.1090506, 2004.

Ni, Y., Foster, G. L., Bailey, T., Elliott, T., Schmidt, D. N., Pearson, P., Haley, B., and Coath, C.: A core top assessment of proxies for the ocean carbonate system in surface-dwelling foraminifers, Paleoceanography, 22, PA001337, https://doi.org/10.1029/2006PA001337, 2007.

Nir, O., Vengosh, A., Harkness, J. S., Dwyer, G. S., and Lahav, O.: Direct measurement of the boron isotope fractionation factor: Reducing the uncertainty in reconstructing ocean paleo-pH, Earth Planet. Sc. Lett., 414, 1–5, https://doi.org/10.1016/j.epsl.2015.01.006, 2015.

Noireaux, J., Mavromatis, V., Gaillardet, J., Schott, J., Montouillout, V., Louvat, P., Rollion-Bard, C., and Neuville, D. R.: Crystallographic control on the boron isotope paleo-pH proxy, Earth Planet. Sc. Lett., 430, 398–407, https://doi.org/10.1016/j.epsl.2015.07.063, 2015.

Pagani, M., Lemarchand, D., Spivack, A., and Gaillardet, J.: A critical evaluation of the boron isotope-pH proxy: The accuracy of ancient ocean pH estimates, Geochim. Cosmochim. Ac., 69, 953–961, https://doi.org/10.1016/j.gca.2004.07.029, 2005.

Palmer, M. R.: Reconstructing past ocean pH-depth profiles, Science, 282, 1468–1471, https://doi.org/10.1126/science.282.5393.1468, 1998.

Palmer, M. R., Spivack, A. J., and Edmond, J. M.: Temperature and pH controls over isotopic fractionation during absorption of boron marine clay, Geochim. Cosmochim. Ac., 51, 2319–2323, https://doi.org/10.1016/0016-7037(87)90285-7, 1987.

Palmer, M. R., Brummer, G. J., Cooper, M. J., Elderfield, H., Greaves, M. J., Reichart, G. J., Schouten, S., and Yu, J. M.: Multi-proxy reconstruction of surface water pCO_2 in the northern Arabian Sea since 29 ka, Earth Planet. Sci. Lett., 295, 49–57, https://doi.org/10.1016/j.epsl.2010.03.023, 2010.

Pearson, P. and Palmer, M.: Middle Eocene seawater pH and atmospheric carbon dioxide concentrations, Science, 284, 1824–1826, 1999.

Pearson, P. N. and Palmer, M. R.: Atmospheric carbon dioxide concentrations over the past 60 million years, Nature, 406, 695–699, doi.org/10.1038/35021000, 2000.

Pearson, P. N., Foster, G. L., and Wade, B. S.: Atmospheric carbon dioxide through the Eocene–Oligocene climate transition, Nature, 461, 1110–1113, doi.org/10.1038/nature08447, 2009.

Penman, D. and Hönisch, B.: Rapid and sustained surface ocean acidification during the Paleocene-Eocene Thermal Maximum, Paleoceanography, 29, 357–369, https://doi.org/10.1002/2014PA002621, 2014.

Rae, J. W. B., Foster, G. L., Schmidt, D. N., and Elliott, T.: Boron isotopes and B : Ca in benthic foraminifera: Proxies for the deep ocean carbonate system, Earth Planet. Sc. Lett., 302, 403–413, https://doi.org/10.1016/j.epsl.2010.12.034, 2011.

Rae, J. W. B., Sarnthein, M., Foster, G. L., Ridgwell, A., Grootes, P. M., and Elliott, T.: Deep water formation in the North Pacific and deglacial CO_2 rise, Paleoceanography, 29, 645–667, https://doi.org/10.1002/2013PA002570, 2014.

Reynaud, S., Hemming, N. G., Juillet-Leclerc, A., and Gattuso, J. P.: Effect of pCO_2 and temperature on the boron isotopic composition of the zooxanthellate coral *Acropora* sp., Coral Reefs, 23, 539–546, https://doi.org/10.1007/s00338-004-0399-5, 2004.

Ries, J. B., Cohen, A. L., and McCorkle, D. C.: Marine calcifiers exhibit mixed responses to CO_2-induced ocean acidification, Geology, 37, 1131–1134, https://doi.org/10.1130/G30210A.1, 2009.

Ries, J. B.: Skeletal mineralogy in a high-CO_2 world, J. Exp. Mar. Bio. Ecol., 403, 54–64, https://doi.org/10.1016/j.jembe.2011.04.006, 2011b.

Ries, J. B.: A physicochemical framework for interpreting the biological calcification response to CO_2-induced ocean acidification, Geochim. Cosmochim. Ac., 75, 4053–4064, https://doi.org/10.1016/j.gca.2011.04.025, 2011a.

Ries, J. B., Ghazaleh, M. N., Connolly, B., Westfield, I., and Castillo, K. D.: Impacts of ocean acidification and warming on the dissolution kinetics of whole-shell biogenic carbonates, Geochim. Cosmochim. Ac., 192, 318–337, https://doi.org/10.1016/j.gca.2016.07.001, 2016.

Rink, S., Kühl, M., Bijma, J., and Spero, H. J.: Microsensor studies of photosynthesis and respiration in the symbiotic foraminifer *Orbulina universa*, Mar. Biol., 131, 583–595, https://doi.org/10.1007/s002270050350, 1998.

Rollion-Bard, C., Chaussidon, M., and France-lanord, C.: pH control on oxygen isotopic composition of symbiotic corals, Earth Planet. Sc. Lett., 215, 275–288, https://doi.org/10.1016/S0012-821X(03)00391-1, 2003.

Rollion-Bard, C. and Erez, J.: Intra-shell boron isotope ratios in the symbiont-bearing benthic foraminiferan *Amphistegina lobifera*: Implications for δ^{11}B vital effects and paleo-pH reconstructions, Geochim. Cosmochim. Ac., 74, 1530–1536, https://doi.org/10.1016/j.gca.2009.11.017, 2010.

Rollion-Bard, C., Chaussidon, M., and France-Lanord, C.: Biological control of internal pH in scleractinian corals: Implications on paleo-pH and paleo-temperature reconstructions, C. R. Geosci., 343, 397–405, https://doi.org/10.1016/j.crte.2011.05.003, 2011a.

Rollion-Bard, C., Blamart, D., Trebosc, J., Tricot, G., Mussi, A., and Cuif, J. P.: Boron isotopes as pH proxy: A new look at boron speciation in deep-sea corals using ^{11}B MAS NMR and EELS, Geochim. Cosmochim. Ac., 75, 1003–1012, https://doi.org/10.1016/j.gca.2010.11.023, 2011b.

Rustad, J. R. and Bylaska, E. J.: *Ab initio* calculation of isotopic fractionation in $B(OH)_3$ (aq) and $B(OH)_4^-$ (aq), J. Am. Chem. Soc., 129, 2222–2223, https://doi.org/10.1021/ja0683335, 2007.

Sanyal, A., Hemming, N. G., Hanson, G. N., and Broecker, W. S.: Evidence for a higher pH in the glacial ocean from boron isotopes in foraminifera, Nature, 373, 234–236, https://doi.org/10.1038/373234a0, 1995.

Sanyal, A., Hemming, N. G., Broecker, W., Lea, W., Spero, J., and Hanson, N.: Oceanic pH control on the boron isotopic composition of foraminifera?: Evidence from culture experiments, Palaeoceanography, 11, 513–517, 1996.

Sanyal, A., Hemming, N. G., Broecker, W. S., and Hanson, G. N.: Changes in pH in the eastern equatorial Pacific across stage 5–6 boundary based on boron isotopes in foraminifera, Global Biogeochem. Cy., 11, 125–133, https://doi.org/10.1029/97GB00223, 1997.

Sanyal, A., Nugent, M., Reeder, R. J., and Bijma, J.: Seawater pH control on the boron isotopic composition of calcite: evidence from inorganic calcite precipitation experiments, Geochim. Cosmochim. Ac., 64, 1551–1555, https://doi.org/10.1016/S0016-7037(99)00437-8, 2000.

Sanyal, A., Bijma, J., Spero, H., and Lea, D. W.: Empirical relationship between pH and the boron isotopic composition of *Globigerinoides sacculifer*: Implications for the boron isotope paleo-pH proxy, Paleoceanography, 16, 515–519, https://doi.org/10.1029/2000PA000547, 2001.

Schoepf, V., McCulloch, M. T., Warner, M. E., Levas, S. J., Matsui, Y., Aschaffenburg, M. D., and Grottoli, A. G.: Short-term coral bleaching is not recorded by skeletal boron isotopes, edited by: C. R. Voolstra, PLoS One, 9, e112011, https://doi.org/10.1371/journal.pone.0112011, 2014.

Short, J. A., Pedersen, O., and Kendrick, G. A.: Turf algal epiphytes metabolically induce local pH increase, with implications for underlying coralline algae under ocean acidification, Estuar. Coast. Shelf S., 164, 463–470, https://doi.org/10.1016/j.ecss.2015.08.006, 2015.

Simkiss, K. and Wilbur, K. M.: Biomineralization: Cell iology and Mineral Deposition, Academic Press, San Diego, 1989.

Spivak, A. J., You, C.-F., and Smith, J.: Foraminiferal boron isotope ratios as a proxy for surface ocean pH over the past 21 Myr, Nature, 363, 149–151, 1993.

Stumpp, M., Hu, M. Y., Melzner, F., Gutowska, M. A., and Dorey, N.: Acidified seawater impacts sea urchin larvae pH regulatory systems relevant for calcification, P. Natl. Acad. Sci. USA, 109, 18192–18197, https://doi.org/10.1073/pnas.1209174109, 2012.

Tambutté, E., Allemand, D., Zoccola, D., Meibom, A., Lotto, S., Caminiti, N., and Tambutté, S.: Observations of the tissue-skeleton interface in the scleractinian coral *Stylophora pistillata*, Coral Reefs, 26, 517–529, https://doi.org/10.1007/s00338-007-0263-5, 2007.

Trotter, J., Montagna, P., McCulloch, M., Silenzi, S., Reynaud, S., Mortimer, G., Martin, S., Ferrier-Pagès, C., Gattuso, J. P., and Rodolfo-Metalpa, R.: Quantifying the pH "vital effect" in the temperate zooxanthellate coral *Cladocora caespitosa*: Validation of the boron seawater pH proxy, Earth Planet. Sc. Lett., 303, 163–173, https://doi.org/10.1016/j.epsl.2011.01.030, 2011.

Uchikawa, J., Penman, D. E., Zachos, J. C., and Zeebe, R. E.: Experimental evidence for kinetic effects on B : Ca in synthetic calcite: Implications for potential $B(OH)_4^-$ and $B(OH)_3$ incorporation, Geochim. Cosmochim. Ac., 150, 171–191, https://doi.org/10.1016/j.gca.2014.11.022, 2015.

Vengosh, A., Kolodny, Y., Starinsky, A., Chivas, A. R., and McCulloch, M. T.: Coprecipitation and isotopic fractionation of boron in modern biogenic carbonates, Geochim. Cosmochim. Ac., 55, 2901–2910, https://doi.org/10.1016/0016-7037(91)90455-E, 1991.

Venn, A. A., Tambutté, E., Lotto, S., Zoccola, D., Allemand, D., and Tambutté, S.: Imaging intracellular pH in a reef coral and symbiotic anemone, P. Natl. Acad. Sci. USA, 106, 16574–16579, https://doi.org/10.1073/pnas.0902894106, 2009.

Venn, A., Tambutté, E., Holcomb, M., Allemand, D., and Tambutté, S.: Live tissue imaging shows reef corals elevate pH under their calcifying tissue relative to seawater, PLoS One, 6, e20013, https://doi.org/10.1371/journal.pone.0020013, 2011.

Venn, A. A., Tambutté, E., Holcomb, M., Laurent, J., Allemand, D., and Tambutté, S.: Impact of seawater acidification on pH at the tissue-skeleton interface and calcification in reef corals, P. Natl. Acad. Sci. USA, 110, 1634–1639, https://doi.org/10.1073/pnas.1216153110, 2013.

Wall, M., Fietzke, J., Schmidt, G. M., Fink, A., Hofmann, L. C., de Beer, D., and Fabricius, K. E.: Internal pH regulation facilitates in situ long-term acclimation of massive corals to end-of-century carbon dioxide conditions, Sci. Rep., 6, 30688, https://doi.org/10.1038/srep30688, 2016.

Wang, B.-S., You, C.-F., Huang, K.-F., Wu, S.-F., Aggarwal, S. K., Chung, C.-H., and Lin, P.-Y.: Direct separation of boron from Na-and Ca-rich matrices by sublimation for stable isotope measurement by MC-ICP-MS, Talanta, 82, 1378–1384, 2010.

Wei, G., McCulloch, M. T., Mortimer, G., Deng, W., and Xie, L.: Evidence for ocean acidification in the Great Barrier Reef of Australia, Geochim. Cosmochim. Ac., 73, 2332–2346, https://doi.org/10.1016/j.gca.2009.02.009, 2009.

Weiner, S., Traub, W., and Parker, S. B.: Macromolecules in mollusc shells and their functions in biomineralization, Philos. Trans. R. Soc. B, 304, 425–434, https://doi.org/10.1098/rstb.1984.0036, 1984.

Wheeler, A.: Mechanisms of molluscan shell formation, in: Calcification in biological systems, edited by: Bonucci, E., CRC Press, 179–216, 1992.

Wilbur, K. and Saleuddin, A.: Shell formation, in: The Mollusca, edited by: Wilbur, K. and Saleuddin, A., Academic Press, 235–287, 1983.

Xiao, J., Jin, Z. D., Xiao, Y. K., and He, M. Y.: Controlling factors of the δ^{11}B-pH proxy and its research direction, Environ. Earth Sci., 71, 1641–1650, https://doi.org/10.1007/s12665-013-2568-8, 2014.

Yu, J., Foster, G. L., Elderfield, H., Broecker, W. S., and Clark, E.: An evaluation of benthic foraminiferal B / Ca and δ^{11}B for deep ocean carbonate ion and pH reconstructions, Earth Planet. Sc. Lett., 293, 114–120, https://doi.org/10.1016/j.epsl.2010.02.029, 2010.

Yu, J., Thornalley, D. J. R., Rae, J. W. B., and McCave, N. I.: Calibration and application of B / Ca, Cd / Ca, and δ^{11}B in *Neogloboquadrina pachyderma* (sinistral) to constrain CO_2 uptake in the subpolar North Atlantic during the last deglaciation, Paleoceanography, 28, 237–252, https://doi.org/10.1002/palo.20024, 2013.

Zeebe, R. E.: Stable boron isotope fractionation between dissolved $B(OH)_3$ and $B(OH)_4^-$, Geochim. Cosmochim. Ac., 69, 2753–2766, https://doi.org/10.1016/j.gca.2004.12.011, 2005.

Zeebe, R. E. and Wolf-Gladrow, D.: CO_2 in seawater: Equilibrium, kinetics, isotopes, New York, Elsevier, 360 pp., 2001.

Zeebe, R. E. and Sanyal, A.: Comparison of two potential strategies of planktonic foraminifera for house building: Mg^{2+} or H^+ removal?, Geochim. Cosmochim. Ac., 66, 1159–1169, https://doi.org/10.1016/S0016-7037(01)00852-3, 2002.